ELSEVIER

Journal of Volcanology and Geothermal Research 101 (2000) 129–154

Journal of volcanology and geothermal research

www.elsevier.nl/locate/jvolgeores

Aso94: Aso seismic observation with broadband instruments

H. Kawakatsu[a,*], S. Kaneshima[b], H. Matsubayashi[a], T. Ohminato[c], Y. Sudo[d], T. Tsutsui[d], K. Uhira[e], H. Yamasato[f], H. Ito[c], D. Legrand[a]

[a]*Earthquake Research Institute, University of Tokyo, 1-1-1 Yayoi, Bunkyo-ku, Tokyo 113, Japan*
[b]*Faculty of Sciences, Tokyo Institute of Technology, O-Okayama, Meguro-ku, Tokyo, Japan*
[c]*Geological Survey of Japan, Higashi, Tsukuba 305, Japan*
[d]*Aso Volcanological Laboratory, Faculty of Science, Kyoto University, Aso, Kumamoto 869-14, Japan*
[e]*Japan Meteorological Agency, Tokyo 110, Japan*
[f]*Meteorological Research Institute, Tsukuba 305, Japan*

Received 21 September 1998; received in revised form 26 April 1999; accepted 26 July 1999

Abstract

We deployed a network of broadband seismometers for one year around the Naka-dake first crater of Aso volcano in Kyushu, Japan, to reveal the mechanism of long period tremors (LPTs) emitted from the volcano. It is observed that LPTs with a dominant period of about 15 s are always emitted regardless of the surface activity of the volcano. A typical LPT has a short duration less than a minute and its spectrum shows mode peaks at 15, 7.5, 5, and 3 s. The particle motion in the frequency band for the lowest two modes at stations within a few kilometers from the crater is rectilinear, pointing in the direction of the crater. A waveform semblance technique to locate sources of LPTs is devised to utilize the rectilinearity of waveforms. The LPT sources are located at depths of 1–1.5 km beneath the bottom of the crater. When the volcano is explosively ejecting steam and mud, on the other hand, a very long period (∽100 s) displacement (VLPD) polarized outward from the crater often precedes an eruptive event by a few minutes. A typical VLPD is accompanied by a few long period pulses, first positively polarized and concurrent with the onset of VLPD, then negatively polarized just before the eruption. The source of VLPDs is inferred to coincide approximately with that of LPT. On the basis of these observations, a qualitative model is constructed for the hydrothermal system beneath the Naka-dake first crater. An explanation for the unusually long period nature of the LPT is discussed in terms of a class of slow waves, which exist in solid–liquid two-phase systems. A possibility of realtime monitoring at Aso volcano using the observed long period seismic signals is also discussed. © 2000 Elsevier Science B.V. All rights reserved.

Keywords: broadband seismometer; volcanic tremor; Aso volcano; crack; hydrothermal system; slow wave; crack wave; semblance; phreatic eruption

1. Introduction

Seismic events occurring near active volcanoes often have distinct characteristics, which are quite different from those of ordinary tectonic earthquakes. They are thus often classified as volcanic earthquakes or volcanic tremors (Minakami, 1960). The occurrence of volcanic tremor is considered to reflect underground movement of fluids such as magma. Tremor is also associated with processes in which

* Corresponding author. Tel.: + 81-3-5841-5817; fax: + 81-3-3812-9417.
E-mail address: hitosi@eri.u-tokyo.ac.jp (H. Kawakatsu).

0377-0273/00/$ - see front matter © 2000 Elsevier Science B.V. All rights reserved.
PII: S0377-0273(00)00166-9

materials such as magma, fragmented rocks, water, and steam are ejected explosively from the crater. The origin of volcanic tremor has long attracted the interest of many volcano seismologists. A number of physical models, including hydrothermal boiling in ground water flow channels (Leet, 1988), harmonic oscillation of a spherical magma chamber (Kubotera, 1974; Crosson and Bame, 1987), oscillation of a cylinder-like magma conduit (Chouet, 1985; McNutt, 1986), and resonance of a fluid-filled crack induced by brittle fracture of the crack (Aki et al., 1977; Chouet, 1986) have been proposed to explain the occurrence of volcanic tremors, but none appears to be conclusive. We understand the properties of resonation with various shapes (spheres, cylinders, cracks), but we do not have a clear understanding of the driving mechanisms. They are most likely non-linear self-excitation mechanisms associated with fluid dynamics.

One of the difficulties in understanding the origin of volcanic tremors and physical mechanisms of the system operating under the volcanic edifices seems to come from the lack of long period seismic data which may illuminate mass advection processes as a whole, or the associated dynamic pressure changes within volcanoes during volcanic activities. Activity of volcanoes has been conventionally monitored with short-period seismometers which record seismic motions only above 1 Hz. Seismometers which are sensitive at longer-period have existed for a long time, but their operation was not so easy at volcanoes. Sassa (1935) installed long-period seismometers at Aso volcano in Kyushu, Japan, 70 years ago to reveal the presence of long-period (3.5–8 s) volcanic tremor. Recent advances in seismometry have now made such observations much easier; portable equipment covering a wide-frequency band (50–0.01 Hz) (Wielandt and Steim, 1986) can be easily installed at volcanoes (e.g. Kawakatsu et al., 1992; Hellweg et al., 1994; Neuberg et al., 1994), and the broadband nature of volcanic activity is becoming clear (e.g. Kaneshima et al., 1996; Ohminato and Ereditato, 1997; Ohminato et al., 1998; Rowe et al., 1998).

In the present paper, we report the main results obtained from the Aso94 campaign, in which we deployed a network of broadband seismometers at Aso volcano. This deployment repeated and expanded Sassa's pioneering observations with state-of-the-art equipment. With the current generation of high-sensitivity broadband seismometers, a number of new results were obtained. These include: (1) long-period volcanic tremors with a period near 15 s are observed nearly always even when there is no surface activity at the crater, and their origin appears to be very shallow (~1.5 km); (2) long-period waves (~20 s) generated by small phreatic eruptions can be recognized at remote seismic stations as far as 1200 km away from the volcano; and (3) very long period (>100 s) seismic signals associated with those small eruptions are observed at close-in stations, and combined with the long-period tremor data, they provide us with a vivid image of what is occurring below the crater during the entire process of the explosive events. Some of these results have been reported previously either in the Japanese language as a thesis (Matsubayashi, 1995), or in a short letter (Kaneshima et al., 1996). The full description of the observations, however, will be given below for the first time.

1.1. Nomenclature

Before going into the detail of the observations, to avoid confusion, few words seem necessary on the nomenclature of the period of waves used in this paper. Following our earlier report (Kaneshima et al., 1996), we use a term "long-period" for periods substantially longer than 1 s, and we use "short-period" for periods shorter than 1 s. This convention is different from those based on recordings of short-period seismometers (e.g. Chouet, 1996), in which volcanic seismic events of about 1 s are called "long-period events"[1]. Considering the essential broadband nature of the volcanic activities as is shown below, our convention seems more appropriate to describe the observations based on broadband seismometers. A similar convention is also used by Neuberg et al. (1994) who installed broadband seismometers at Stromboli.

2. Broadband seismometry at active volcanoes

2.1. Sassa (1935)

In May of 1929, Kenzo Sassa of Kyoto Imperial

[1] It seems more natural to use a term "low-frequency" (e.g. Hasegawa and Yamamoto, 1994).

University installed Wiechert horizontal component seismographs of 1000 kg (pendulum period $T_0 =$ 10.0 s) and vertical one of 1300 kg ($T_0 = 4.6$ s) in the basement of Aso Volcanological Laboratory (AVL), situated about 7.3 km west of the crater. He also installed Galitzin seismographs ($T_0 = 8.0$ s) and short-period seismographs ($T_0 = 0.55$ s), thus Aso volcano became the first site of broadband seismic observation at an active volcano.

Summarizing the subsequent observations over several years (including some major eruptions), Sassa (1935) classified volcanic seismic signals of Aso into four different kinds of tremors, as well as "eruption-earthquakes". They are "the volcanic micro-tremors of the first kind" (period of 0.8–1.5 s), "the second kind" (3.5–8.0 s), "the third kind" (0.4–0.6 s), and "the fourth kind" (0.2 s). The observation of these tremors in the wide-frequency band ranging from 0.2 to 8.0 s clearly demonstrates the efficacy of broadband seismometry at active volcanoes. Analyzing those data, Sassa was able to infer a possible presence of "a magmatic reservoir of gas-riched magma" immediately beneath the crater at a depth of about 1 km. He also suggested the presence of cracks in the direction of the chain of the craters.

Since Sassa's pioneering work, there have been few published reports on attempts to observe long-period volcanic seismic signals until recently, when it has become much easier to install portable broadband instruments. Seidl et al. (1981) installed broadband seismometers at Etna, Italy and observed 4–5 s period signals, which they suggested as one of the fundamental peaks of the Etna tremors. They also note that tremor signal of 3 s was suggested by Caloi et al. (1948). Churei (1985) installed two intermediate-period seismometers at Aso in order to observe Sassa's second kind of tremors. He showed that the period of the tremor can be as long as 10 s, and the source is located in the same general area that Sassa inferred.

Examples of deployments of the current generation broadband seismometers are now plentiful: e.g. Sakurajima, Japan (Kawakatsu et al., 1992, 1994), Unzen, Japan (Yamasato et al., 1993; Uhira et al., 1994b), Stromboli, Italy (Dreier et al., 1994; Falsaperla et al., 1994; Neuberg et al., 1994), Semeru, Java (Hellweg et al., 1994), Aso, Japan (Kaneshima et al., 1996; this paper), Kilauea, USA (Ohminato et al., 1998), Satsuma-Iwojima, Japan (Ohminato and Ereditato, 1997), Arenal, Costa Rica (Hagerty et al., 1997), Erebus, Antarctica (Rowe et al., 1998). A variety of long-period volcanic seismic signals have been observed at different volcanoes, and a new class of volcano seismology appears to be emerging. Different physics apply at different frequencies, and this makes volcanic seismic signals essentially broadband.

2.2. Studies of long-period volcanic signals

Long-period volcanic signals have also been recorded by seismic networks of regional and/or global scales, and analyzed by various researchers. One of the advantages of using such long-period signals is that they provide for waveform analysis to infer excitation mechanisms more easily than do short-period seismograms. Kanamori and Given (1982) modeled the long-period seismic signals accompanied with the eruption of the Mt. St. Helens in 1980 recorded at stations of the global seismic networks (GDSN, IDA). They showed that the so-called single force mechanism can explain the radiation pattern of long-period surface waves, and attributed it to the gigantic mass movement of the volcano edifice due to the landslide. Kanamori et al. (1984) also analyzed the long-period bodywaves generated by the same eruption, and showed that vertical single forces due to the depressurization of the magma chamber explains the data. With these two single force mechanisms, they could vividly picture what had occurred during the whole sequence of the eruption. These two studies inspired further applications of long-period seismology to study volcanic activities.

The general source description for long-period signals using moment tensor and single force has become common in seismological studies of volcanic activities. Examples of such studies include the following: Asama-yama, Japan (Takeo et al., 1984), Long Valley, USA (Julian, 1983; Aki, 1984; Julian and Sipkin, 1985; Wallace, 1985), O-shima, Japan (Fukuyama and Takeo, 1990; Takeo et al., 1990), Sakurajima, Japan (Uhira and Takeo, 1994), Unzen, Japan (Yamasato et al., 1993; Uhira et al., 1994b), Kilauea, Hawaii (Eissler and Kanamori, 1987; Kawakatsu, 1989; Ohminato et al., 1998), Mt. St. Helens (Kanamori and Given, 1982; Kanamori et al., 1984;

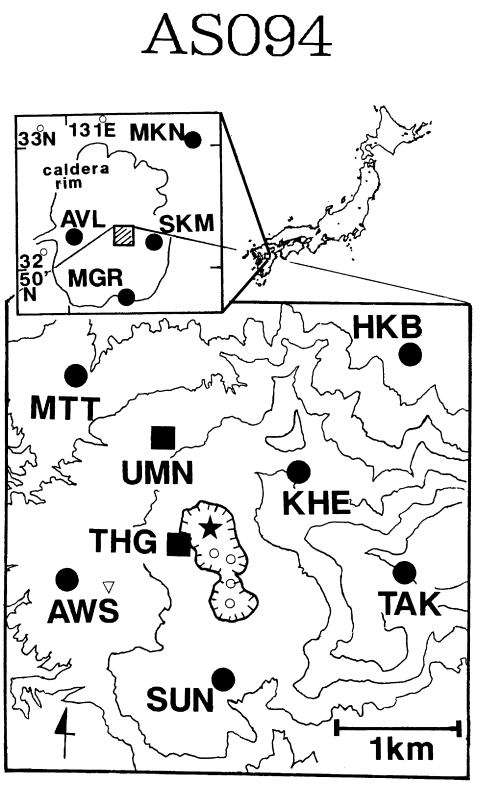

Fig. 1. Station map: Aso volcano is an andesitic volcano located in the middle of Kyushu, Japan. Filled circles: stations operated for 1 year. Filled squares: temporary stations operated for 8 days in November. Eight of the 12 stations are around the Nakadake first crater (star) on the central cone (shaded square in inset). The other four stations are near the outer rim of the caldera (solid line in inset). A NNW–SSE trending chain of older craters is indicated by small open circles. Topography near the craters is shown with contours with an interval of 100 m. A microbarograph was installed 300 m east of station AWS (open triangle).

Kawakatsu, 1989), Ito-oki, Japan (Takeo, 1992), Torishima, Japan (Kanamori et al., 1993), Iceland (Julian and Foulger, 1996; Nettles and Ekstrom, 1998). Applications of such analysis techniques for shorter-period (~1 s) near-field records obtained at volcanoes are also becoming available (Uhira et al., 1994a; Nishimura et al., 1995; Ohminato, 1997). Long-period volcanic signals recorded at volcanoes with broadband instruments should thus be easily incorporated into routine analyses to infer their excitation mechanisms. Further general description of source as Takei and Kumazawa (1995) may also become applicable using such data.

2.3. Aso94 campaign

2.3.1. The network

From April 1994 to March 1995, we installed 10 broadband three-component velocity seismometers with a free period of 120 s (STS2) or 30 s (CMG3T) around Aso volcano in Kyushu, Japan (Fig. 1). This campaign was conducted as a cooperative project among different universities and national institutes in Japan. In November 1994, two additional seismometers (CMG3T with a 100 s free period) were also temporarily deployed near the crater for 8 days to improve the azimuth and distance coverage of stations relative to the crater. Seismic signals were recorded continuously with portable data loggers either on digital tapes, hard disks, or magneto-optical disks, with the sampling rate of 20 Hz and with the dynamic range of either 16 or 24 bits. Clocks of the recorders were either locked with GPS or adjusted by radio time signals, so that timing is accurate enough for the later analyses of long-period signals. Eight of the 12 stations were located within 2.5 km from the center of the Naka-dake first crater realizing a good azimuthal coverage (Fig. 1). Further details of the network are given in Table 1.

2.3.2. Activity of Aso volcano

The activity of Aso volcano changes from time to time. The changing pattern of the surface activity of the Aso Nakadake first crater is schematically illustrated in Fig. 2. The actual occurrence does not necessarily follow this figure sequentially. Activity leading to a Strombolian eruption may be expected every 5–10 years. It should be noted that our one year of observation covers only a relatively quiet period; the crater has been covered with water of the temperature of ~70°C throughout the observation period.

3. Long-period seismic signals observed at Aso

3.1. Long-period volcanic tremor (LPT)

At Aso volcano, it has long been observed that unusually long period tremor is emitted from the Naka-dake first crater on the central cone (Sassa's

Table 1
Network information

Station	Sensor	Recorder	Recording medium	Sampling frequency (Hz)	Latitude (deg)	Longitude (deg)	Elevation (km)
AVL	Streckeisen STS-2	Teledyne PDAS-100 (16bit)	HD	20	32.882	131.009	0.57
AWS	Guralp CMG-3	NFPCM 5881 (16bit)	DAT	50	32.877	131.075	1.14
HKB	Guralp CMG-3	Teledyne PDAS-100 (16bit)	HD	20	32.893	131.103	0.98
KHE	Streckeisen STS-2	Columbia DTC 8000 (16bit)	MO	20	32.886	131.095	1.28
MTT	Streckeisen STS-2	Reftek Tarraprobe (24bit)	DAT	20	32.895	131.064	1.02
SKM	Streckeisen STS-2	Teledyne PDAS-100 (16bit)	HD	20	32.871	131.137	0.77
SUN	Streckeisen STS-2	Reftek Tarraprobe (24bit)	DAT	20	32.870	131.089	1.24
TAK	Streckeisen STS-2	Reftek Tarraprobe (24bit)	DAT	20	32.878	131.102	1.45
MGR	Guralp CMG-3	Columbia DTC 8000 (16bit)	MO	20	32.796	131.093	0.68
MKN	Streckeisen STS-2	Columbia DTC 8000 (16bit)	MO	20	33.009	131.199	0.67
THG	Guralp CMG-3	Teledyne PDAS-100 (16bit)	HD	20	32.881	131.085	1.27
UMN	Guralp CMG-3	Teledyne PDAS-100 (16bit)	HD	20	32.888	131.083	1.18
1st crater					32.881	131.086	1.16

"second kind" of tremor, called LPT for simplicity hereafter) (Sassa, 1935). A typical LPT has a short duration less than a minute, and may rather be called an event than a tremor. The occurrence of LPT has been repeatedly reported since Sassa's work (Churei, 1985; Hashida, 1990), but those observations have fallen short of unraveling the origin of LPT as well as the location, size and geometry of the LPT source, because of the limited number of instruments near the crater.

3.1.1. LPT waveform

In the observed raw broadband seismograms, shorter period volcanic tremors such as Sassa's "first (~1 s) and third (~0.5 s) kind" tremors and/or microseisms generated by oceanic waves (period 4–6 s) usually dominate. LPTs are most clearly visible as a series of isolated wave packets of a few cycles on filtered seismograms with the passband of 10–30 s. Fig. 3 shows examples of LPTs observed at the station TAK. During most of our observation period (cf. Fig. 2) Aso was inactive, exhibiting no major surface activity at the crater, yet LPTs were ubiquitously observed.

Fig. 3 illustrates changing patterns of LPT activity over time. The pattern shown in Fig. 3a was recorded at the beginning of the campaign, and appears to be most common: isolated events with relatively large amplitude (~0.5 μm/s) are observed rather randomly. This pattern was followed by the one in Fig. 3b: LPTs are still present but with a very small amplitude (LPT activity as low as this was observed only during this period). On June 7, 1994 (Fig. 3c) a rhythmical pattern began with fairly constant interval of LPT occurrences. This then transformed into almost continuous LPT. This transition was clearly observed within a few hours on June 7, 1994, as a gradual decrease in the interval between discrete LPT occurrences. Some

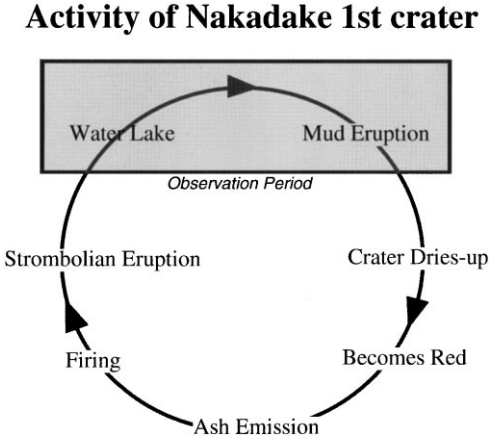

Fig. 2. The changing pattern of the surface activity of the Aso Nakadake first crater is schematically summarized. The actual occurrence does not necessarily follow this figure sequentially. Activity leading to an Strombolian eruption may be expected every 5–10 years. Note that our observation period covers a very quite period of the volcano, during which no magmatic eruptions occurred.

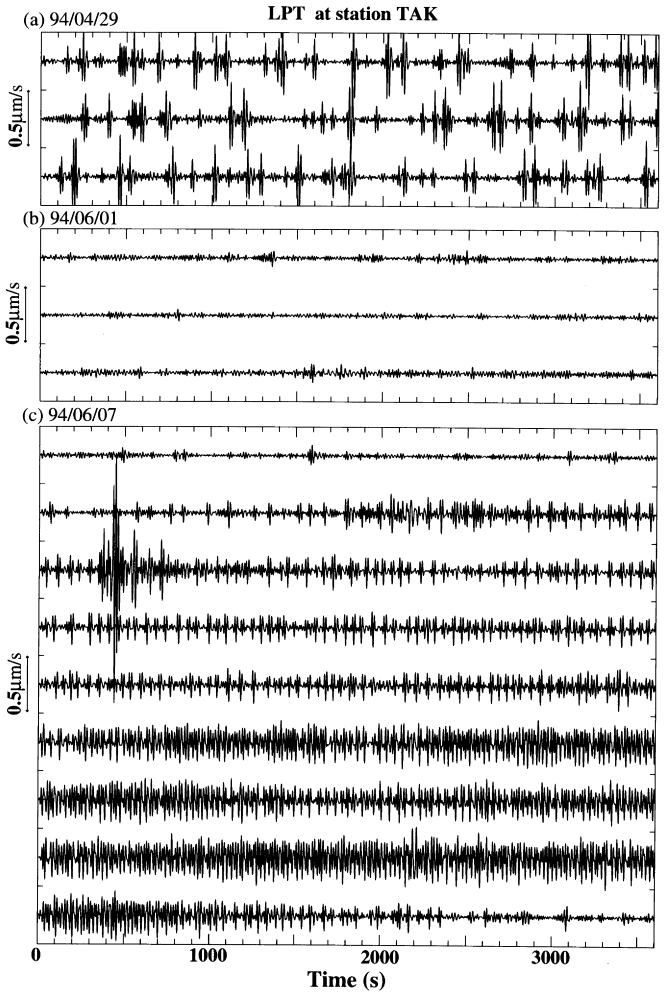

Fig. 3. Vertical component band-pass filtered (10–30 s) velocity seismograms at station TAK are shown for three different days: (a) 3 h starting at ∽18:20 on April 29; (b) 3 h starting at ∽00:08 on June 1; (c) 9 h starting at ∽07:14 on June 7. Tick marks on the horizontal axes indicate 100 s, and the horizontal scale is 1 h. The large amplitude signal in (c) is due to a remote earthquake. Signals above a amplitude of 0.1 μm/s all correspond to LPTs. Although amplitude is small in (b), the stacked spectrum similar to Fig. 6 shows consistent mode peaks, suggesting that LPTs are present even in this record.

similarity exists between the LPT occurrence and the seismicity at geyser (Kieffer, 1984). The relation between LPT and shorter period tremors seems not simple. LPT is occasionally accompanied by short-period tremor ("first kind") at the onset (Sassa, 1935; Kikuchi, 1974), as if the shorter event triggered the LPT.

Fig. 4 shows an example of vertical displacement waveforms of typical LPTs observed at different stations. The waveforms at the different stations are almost identical. This is because these long-period signals observed in the near-field mainly consist of the static displacement (Legrand et al., 2000 – this issue). Waveforms are highly repeatable from event to event with a dominant period of about 15 s, suggesting a repetitive, non-destructive source mechanism.

3.1.2. LPT particle motion

When the static displacement dominates in the near field, waveforms are similar on the three components.

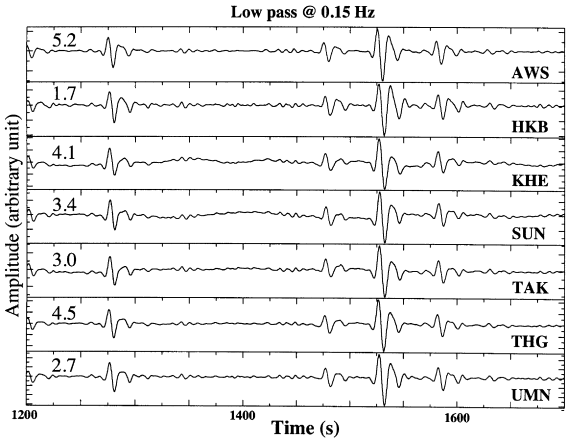

Fig. 4. Vertical component low-pass filtered (0.15 Hz) velocity seismograms at the seven close-in stations. Seismograms start at 07:20 on November 23. Each seismogram is scaled by its maximum to show the similarity of the waveform to one another. The peak-to-peak amplitude is indicated at the upper-left in units of μm/s.

Hence, the polarization becomes rectilinear, pointing to the source direction, and the signal appears like P waves (Legrand et al., 2000 – this issue). This is a common feature of many long-period signals observed at volcanoes (Sassa, 1935; Churei, 1985; Neuberg et al., 1994; Kaneshima et al., 1996; Ohminato and Ereditato, 1997; Ohminato et al., 1998; Rowe et al., 1998). At most stations near the crater except for UMN, particle motions of LPT in the horizontal planes of the 10–30 s bandpassed seismograms are rectilinear and point approximately to the first crater (Fig. 5a–g). Further, as seen on the particle motions in the vertical–radial plane, incident angles of the LPT observed at most stations around the crater are rather shallow and range approximately from 35 to 75° except for THG and UMN where the incident angles appear to be steeper. In these plots, the positive radial direction is taken as a general direction toward the first crater which also corresponds to the maximum direction of the particle motion in the horizontal plane; If the origin of LPTs is located right beneath the first crater, particle motions in the vertical–radial plane at all stations should show radial–downward patterns. Although this is the case for the most stations, the pattern at the closest station THG is opposite (Fig. 5f). This indicates that the source location is not right beneath the crater but slightly south-west of the crater.

Fig. 5h shows the particle motion of LPT at station TAK around 7.5 s period. The particle motion is rectilinear and essentially the same as that around 15 s period (Fig. 5e). The similar observation applies to the other station records, although in general the rectilinearity at 7.5 s is weaker than that at 15 s.

3.1.3. LPT spectrum

Fig. 6a shows velocity amplitude spectra at three stations (TAK, HKB, MTT) obtained by stacking many spectra. The general features on the stacked spectrum are also visible on the individual ones, although there is much larger noise. As stated above, the dominant period of LPT is approximately 15 s, corresponding to a very stable spectral peak around this period. The observed spectra also show the presence of other consistent long-period peaks at 7.5, 5 and 3 s. Microseisms exhibit a broader hill in the spectra from 2 to 5 s superimposed on these peaks. The attenuation quality factor (Q) corresponding to the 15 s peak of LPT is estimated to be on the order of 5 from the width of spectral peak and from the fact that the oscillation virtually disappears on the bandpassed seismograms 10–30 s after 2 or 3 cycles.

The spectral peaks at 7.5, 5, and 3 s apparently correspond to second, third, and fifth overtones of the harmonic oscillation with the fundamental mode of 15 s stated above. The presence of overtones suggests that LPT result from oscillation of a resonator. Sassa's "second kind" tremor with a dominant period of 3–8 s may actually be the higher modes we observed. Sassa (1935) and Kubotera (1974) reported temporal change of the dominant period of LPT, in concordance with the surface activity of the volcano. There is, however, no significant change in the dominant period of LPT during a year of our observation. Fig. 6b shows the broadband time-frequency diagram (spectrogram) of the vertical component velocity seismogram at the station SUN for the entire period (9 months) of observation. Long-period mode peaks can be seen as horizontally continuous bright colored belts.

3.1.4. LPT source

The onset of a LPT is usually not clearly identified on individual seismograms, hence

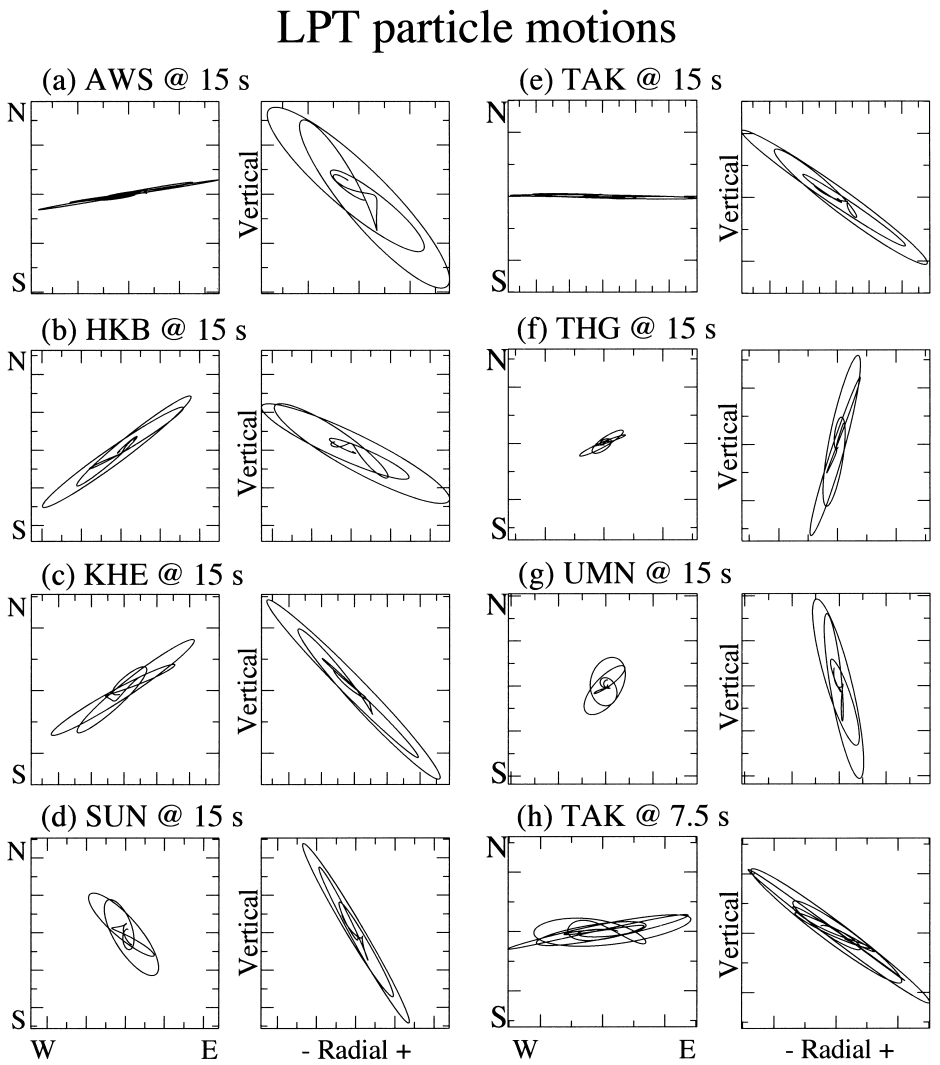

Fig. 5. Particle motions of the band-pass filtered LPT in Fig. 4 (the largest amplitude event around 07:30, November 23). (a)–(g) a 10–30 s filter is applied to seven close-in station records to see the fundamental mode. (h) a 6.7–10 s filter is applied to the TAK record to see the first overtone at 7.5 s. (left): particle motions in the horizontal plane. (right): particle motions in the vertical plane containing the station and the first crater. In these plots, the positive radial direction is taken as a general direction toward the first crater which also corresponds to the maximum direction of the particle motion in the horizontal plane.

conventional approaches of event location by picking first arrivals cannot be applied. As described in the previous section, however, the LPT particle motions are rectilinear and appear to point to a rather narrow region beneath the first crater. Considering that the inclinations are around 45° at stations a few kilometers away from the crater (Fig. 5a–e), the source depth should not exceed a few kilometers. Assuming that the source of LPT is isotropic as a first-order approximation, we developed a technique to locate a LPT from waveform data.

3.1.5. Waveform semblance method

The method is based on the semblance method (Neidel and Tarner, 1971), which has been extensively used to locate either seismic events or point scatterers

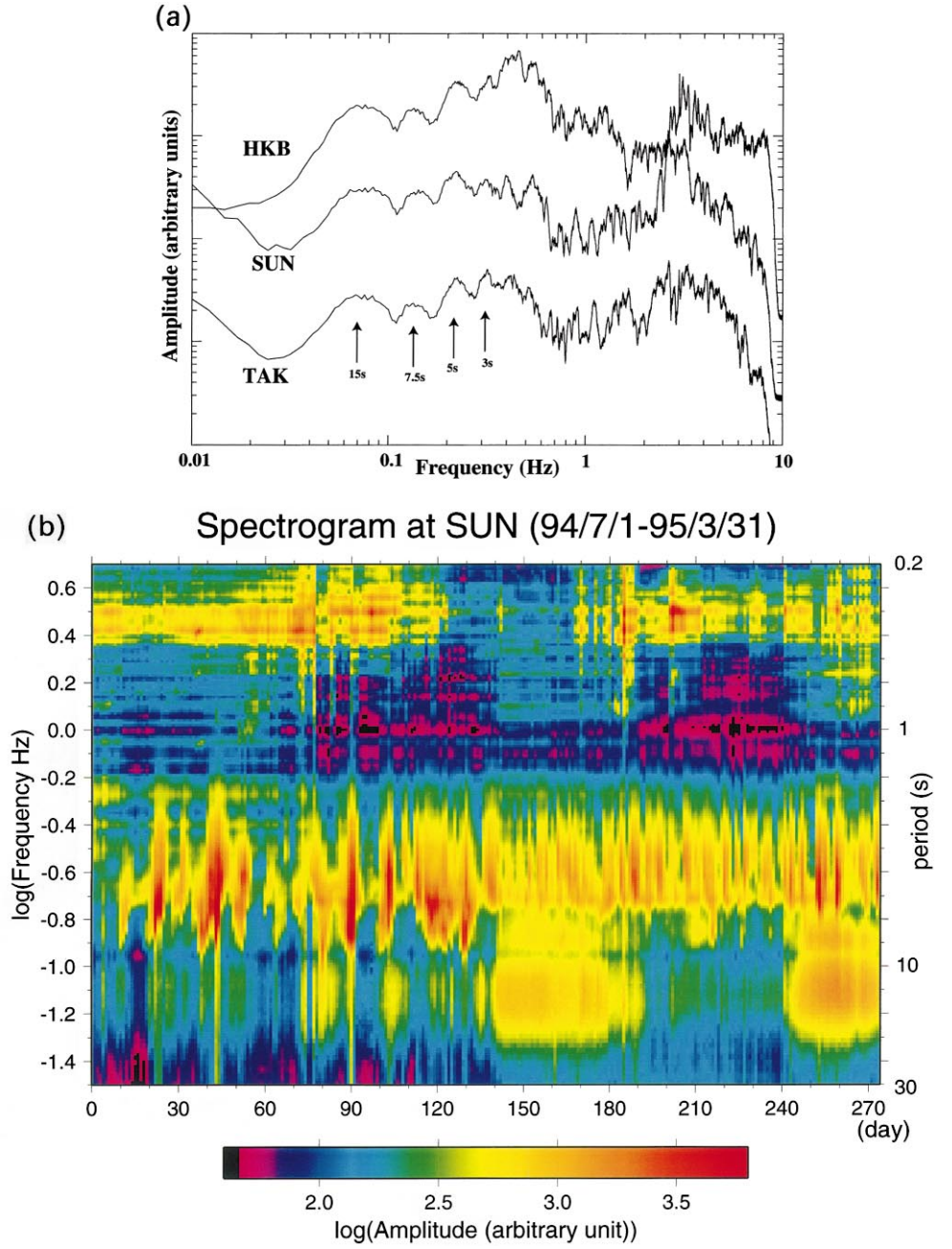

Fig. 6. (a) Amplitude spectra of LPT for stations, TAK, SUN, and HKB, obtained by the stacking of 24-h data of July 27. FFT spectra for 5-min long vertical component raw velocity seismograms are first calculated for a single day at each station, and they are stacked to produce an averaged spectrum. Arrows indicate the identified lowest four mode peaks. (b) Spectrogram at station SUN for a period from 1994/7/1 to 1995/3/31. A spectrum for each day is constructed in the same way as for (a). Teleseismic signals (noises) are removed manually as much as possible. Note that the vertical (frequency) axis is logarithmic to accommodate the broadband nature of the data.

(e.g. Furumoto et al., 1990; Kuwahara et al., 1997). It measures the coherency among seismograms as:

$$S = \frac{\sum_{j=1}^{L}\left(\sum_{i=1}^{N} u_{i,j(i)}\right)^2}{N\sum_{j=1}^{L}\sum_{i=1}^{N} u_{i,j(i)}^2}, \tag{1}$$

where N is the number of stations, and $u_{i,j(i)} \equiv u_i(t_i + j\Delta t)$ is a seismogram of ith station at $j(i)$th time sample; the start time t_i is shifted for each station, depending on the assumed source distance (or the slowness vector of a traversing plane wave), and L is the number of time samples which defines the time window.

In case of an isotropic point source, we may choose the radial component (the direction of a station from the source) as a seismogram $u_{i,j(i)} \equiv R_{i,j(i)}$ for estimating the semblance, and the time shift t_i is estimated from the travel time of the wave of interest as $t_i = t_{\mathrm{ref}} + r_i/\alpha$, where t_{ref}, r_i, α are reference time, source-station distance, and wave velocity, respectively. In order to incorporate information contained in rectilinearity of the particle motions of our seismograms, we modify the conventional semblance (1) to penalize the departure from the rectilinearity by subtracting the other components as follows:

$$S_3 = \frac{1}{D}\sum_{j=1}^{L}\left\{\left(\sum_{i=1}^{N} R_{i,j(i)}\right)^2 - N\left(\sum_{i=1}^{N} V_{i,j(i)}^2\right) - N\left(\sum_{i=1}^{N} H_{i,j(i)}^2\right)\right\} \tag{2}$$

where V is the component in the direction perpendicular to R within the vertical plane which contains both source and receiver, and H is in the horizontal component perpendicular to both R and V. Note that V is not a vertical component. The scaling factor D can either be:

$$D_1 = N\sum_{j=1}^{L}\sum_{i=1}^{N} R_{i,j(i)}^2, \tag{3}$$

or

$$D_2 = N\sum_{j=1}^{L}\sum_{i=1}^{N} (R_{i,j(i)}^2 + V_{i,j(i)}^2 + H_{i,j(i)}^2). \tag{4}$$

This definition of semblance measures the rectilinearity of particle motion pointing to the source, as well as the coherency of signals. Before applying Eq. (2), each seismogram is normalized such that the RMS amplitude of signal of each station becomes unity: i.e.

$$\mathrm{RMS}_i^2 = \frac{1}{L}\sum_{j=1}^{L}(R_{i,j(i)}^2 + V_{i,j(i)}^2 + H_{i,j(i)}^2) = 1. \tag{5}$$

With this normalization, we effectively remove all the amplitude information contained in the original seismograms. We call the semblance defined by Eq. (2) a "waveform semblance" in the rest of the paper.

The meaning of the waveform semblance can be understood in terms of waveform modeling for an isotropic source as follows. Considering that long-period signals in the near-field mainly consist of static displacements and are proportional to the source time function (Legrand et al., 2000); the best estimate of the source time function may be obtained by averaging radial component seismograms:

$$S_j = \frac{1}{N}\sum_{i=1}^{N} R_{i,j(i)} \qquad (j = 1,\ldots,L), \tag{6}$$

where we assume for simplicity that the stations are equidistant from the source, or that the seismograms are normalized as in Eq. (5). Since there should be no V- and H-components for an isotropic source, the squared residual of the theoretical and observed seismograms will be given by:

$$\sigma^2 = \sum_{i=1}^{N}\sum_{j=1}^{L}(R_{i,j(i)} - S_j)^2 + \sum_{i=1}^{N}\sum_{j=1}^{L} V_{i,j(i)}^2 + \sum_{i=1}^{N}\sum_{j=1}^{L} H_{i,j(i)}^2. \tag{7}$$

Using Eq. (6), this can be expressed further as:

$$\sigma^2 = \sum_{j=1}^{L}\left\{\sum_{i=1}^{N} R_{i,j(i)}^2 - \frac{1}{N}\left(\sum_{i=1}^{N} R_{i,j(i)}\right)^2 + \sum_{i=1}^{N} V_{i,j(i)}^2 + \sum_{i=1}^{N} H_{i,j(i)}^2\right\}. \tag{8}$$

If we normalize this with the power of the whole radial components (the first term of the right-hand side), we get a normalized residual ($\bar{\sigma}^2$) expressed in terms of the waveform semblance:

$$\bar{\sigma}^2 = 1 - S_3, \tag{9}$$

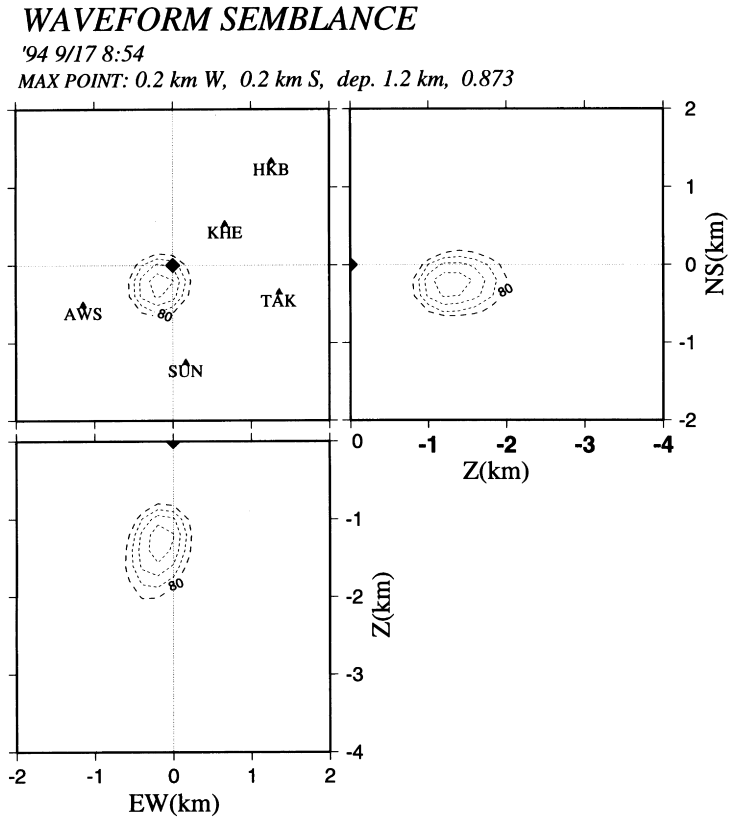

Fig. 7. Estimated point source location for a typical LPT obtained by using the waveform semblance method with an assumption of an isotropic source. Contours indicate semblance values (%) with the interval of 2. Three component seismograms of stations AWS, HKB, KHE, SUN, and TAK are used for this case (cf. Table 2).

where the scaling factor D_1 should be used for obtaining S_3. The waveform semblance is thus a measure of waveform fit for an assumed isotropic point source; when $S_3 = 1$, it means a complete fit of seismograms (i.e. $\sigma = 0$). As a scaling factor in Eq. (2), we use D_2 in stead of D_1, because it appeared to give a better depth resolution in a controlled test of the method (Matsubayashi, 1995). In this case, the waveform semblance takes values between -1 and 1 (i.e. $-1 \leq S_3 \leq 1$), while the conventional one is $0 \leq S \leq 1$.

Fig. 7 shows the result of application of the waveform semblance method to a LPT. Records from five stations are bandpass-filtered around the 15 s peak. A wave velocity of 1.5 km/s is used, because it gives the highest peak semblance value in the tested range between 0.8 and 2.5 km/s (Matsubayashi, 1995). The peak semblance values for LPTs range between 0.85 and 0.89, representing high coherency and strong rectilinearity of the waveforms. The estimated source region is a few hundred meters south-west of the first crater at depths of 1–1.5 km. This location is consistent with the particle motion at THG (Fig. 5f) noted earlier, although data from this station is not used in the analysis. Locations of selected LPTs are listed in Table 2.

3.2. Phreatic eruption and preceding very long-period displacements

Aso volcano became slightly active in September, 1994, and “mud-eruptions”, small phreatic eruptions of mud, water and steam, were visually observed (cf. Fig. 2). A local newspaper reports that the ash and smoke went up as high as 1 km during one eruption

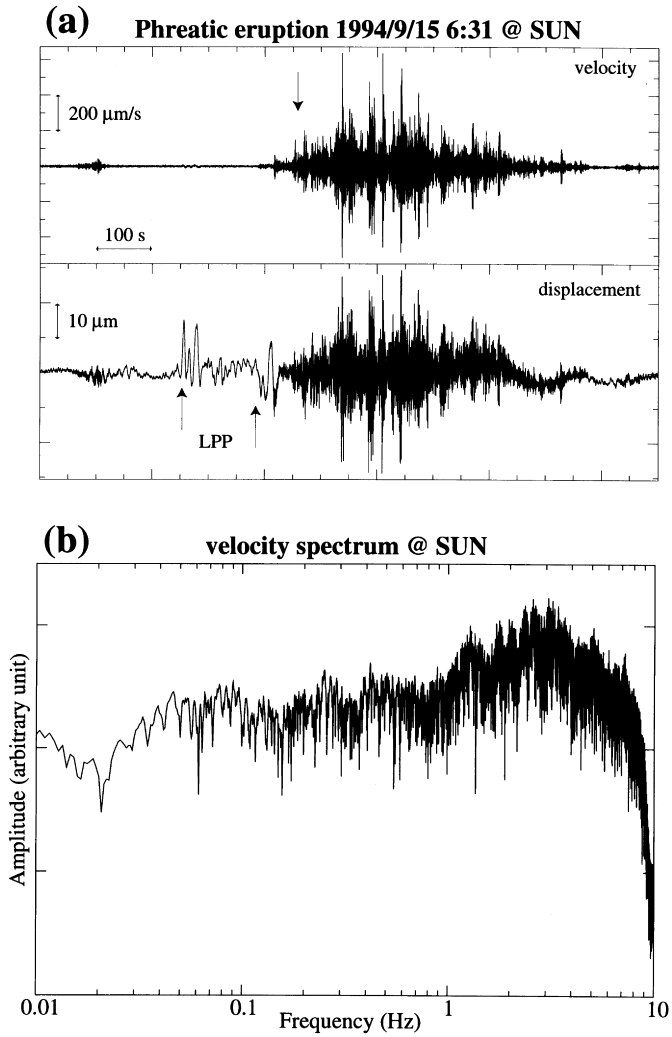

Fig. 8. (a) Phreatic eruption on September 15, 1994 (6:31,GMT) recorded at SUN. (top: raw velocity vertical component; bottom: displacement obtained by a direct integration of the raw record). Downward arrow indicates the onset of the eruption derived by the arrival of the air shock measured by a pressure sensor. This corresponds approximately to the beginning of short period tremor. Long-period pulses (LPPs) indicated by upward arrows precede the eruption. These pulses can be observed at remote seismic stations as far as 1200 km away from Aso (cf. Fig. 17). (b) Spectrum of the velocity record shown in (a). Note the broad peak below 0.1 Hz.

at 6:31 (GMT) on September 15. Fig. 8a shows the vertical component seismograms of the eruption obtained at SUN station. Essential features of the seismograms can be summarized as follows: the onset of short-period tremor corresponds to the time of the reported phreatic eruption (Fig. 8a, top); a positively polarized long-period pulse (LPP) precedes by about 150 s the onset of short-period tremors, which begin when the subsequent negative long-period pulse occurs (Fig. 8a, bottom: displacement seismogram); the time of negative pulse also appears to correspond to the onset of the eruption estimated by the time of the air shock. We note that these features are shared with other phreatic eruptions, regardless of their size.

Fig. 9 compares the particle motion at station TAK for LPTs and a LPP. The particle motion of the LPP is

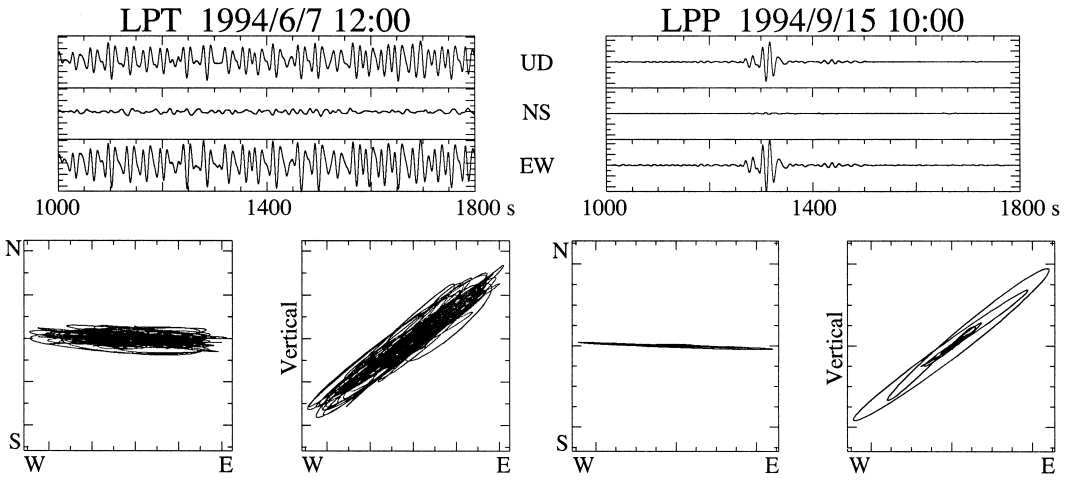

Fig. 9. Comparison of particle motions of LPT and LPP (10–30 s) at station TAK. The particle motions are essentially identical, except for the absolute scale.

Table 2
LPT source location by waveform semblance (locations are given relative to the 1st crater in Table 1)

Date and time	E–W (km)	N–S (km)	Z (km)	Semblance peak value	Station
06/07 10:16	0.0W	0.2S	1.2	0.852	AWS, TAK, HKB
10:18	0.2W	0.2S	1.2	0.853	AWS, TAK, HKB
10:28	0.2W	0.2S	1.2	0.876	AWS, TAK, HKB
11:31	0.2W	0.4S	1.2	0.886	AWS, TAK, HKB
12:17	0.2W	0.2S	1.2	0.876	AWS, TAK, HKB
13:32	0.4W	0.2S	1.0	0.871	AWS, TAK, HKB
07/04 09:27	0.4W	0.4S	1.2	0.846	AWS, TAK, HKB, KHE
10:27	0.2W	0.2S	1.2	0.881	AWS, TAK, HKB, KHE
11:52	0.4W	0.2S	1.2	0.824	AWS, TAK, HKB, KHE
09/17 09:01	0.2W	0.2S	1.2	0.873	AWS, TAK, HKB, SUN, KHE
09:01	0.2W	0.2S	1.2	0.862	AWS, TAK, HKB, SUN, KHE
09:43	0.2W	0.2S	1.2	0.883	AWS, TAK, HKB, SUN, KHE

Table 3
LPP source location by waveform semblance (locations are given relative to the 1st crater in Table 1)

Date and time	E–W (km)	N–S (km)	Z (km)	Semblance peak value	Station
09/15 06:27	0.2W	0.2S	1.2	0.888	AWS, KHE, SUN, TAK
10:00	0.0W	0.4S	1.0	0.965	AWS, KHE, SUN, TAK
10:21	0.2W	0.4S	1.2	0.941	AWS, KHE, SUN, TAK
09/16 19:00	0.2W	0.2S	1.2	0.738	AWS, KHE, SUN, TAK, HKB
09/21 09:56	0.2W	0.2S	1.2	0.933	AWS, KHE, SUN, TAK, HKB
09/22 12:09	0.0W	0.2S	1.2	0.929	AWS, KHE, SUN, TAK, HKB
12:10	0.2W	0.2S	1.4	0.913	AWS, KHE, SUN, TAK, HKB

very similar to that of LPT observed during the inactive period. The waveform semblance analysis also indicates that the source region is the same as that of LPT (Table 3). Despite the apparently similar source locations, spectra for LPPs are not exactly the same as those for LPTs, showing rather broadened features below 0.1 Hz without any consistent sharp peaks among different events (Fig. 8b).

The most remarkable observation associated with phreatic eruptions is the presence of a very long-period (>100 s) displacement (hereafter VLPD) often preceding eruptions by a few minutes (Fig. 10a). Superimposed on the VLPD are the long-period pulses positively polarized at the beginning of the VLPD, then negatively polarized just before the eruption (Fig. 10b). This pattern of VLPD and LPPs seems to be consistent among phreatic eruptions (Fig. 11).

We hypothesize that the VLPD results from a gradual increase in fluid pressure beneath the crater, and we apply models of static deformation due to underground pressure change, to estimate the location of the pressure source as well as the pressure change. We consider a spherical pressure source model (Mogi, 1958). The vertical height of the VLPD is used as data (Fig. 12a). We do not use horizontal components for this analysis because they are less reliable at these long periods. The source location which fits the observed displacements best (Fig. 12b) is 300 m west and 1–1.5 km below the first crater (Table 4). The source location of the phreatic eruption (94/09/21 09:56) estimated by waveform semblance of LPP and by the Mogi model of VLPD are compared in Fig. 13a. Both locations are coincident within the error limits, and are very close to that of LPT. Fig. 13b compares all the locations of LPT, LPP, and VLPD listed in Tables 2 and 3, which are all located in the same general area beneath the crater. Analyzed phreatic eruptions correspond to those shown in Figs. 10 and 11, which have large seismic signals.

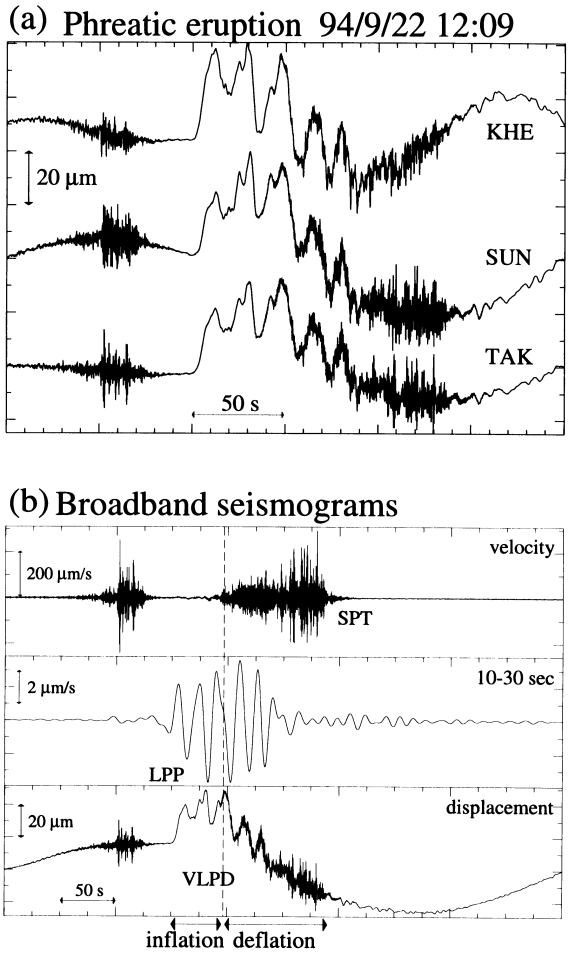

Fig. 10. (a) Very long-period displacement (VLPD) observed at three stations (KHE, SUN, TAK) during a phreatic eruption of 12:09, September 22. The long-period fall-off of the sensitivity of the STS-2 seismometer at 120 s is corrected to obtain displacement seismograms. The very long-period trends of several hundreds seconds are due to noise. Discarding these trends by eye, note that the displacements are mostly positively polarized. (b) Broadband seismograms (vertical component) of the same phreatic eruption observed at TAK: (top) raw velocity seismogram; (middle) velocity seismogram bandpass filtered between 10 and 30 s. LPPs dominate in this frequency range; (bottom) the same displacement shown in (a). The vertical broken line indicates the time of the eruption. A simple and straightforward interpretation of these seismograms is given in Section 4.

3.2.1. Eruption size

The pressure build-up in the LPT source region prior to the phreatic eruptions can be estimated for the assumed spherical sources. In the spherical source model of Mogi (1958), surface displacements are proportional to a "volume change" of the source which is given by:

$$\Delta V = \frac{\pi R^3 \Delta P}{\mu}, \tag{10}$$

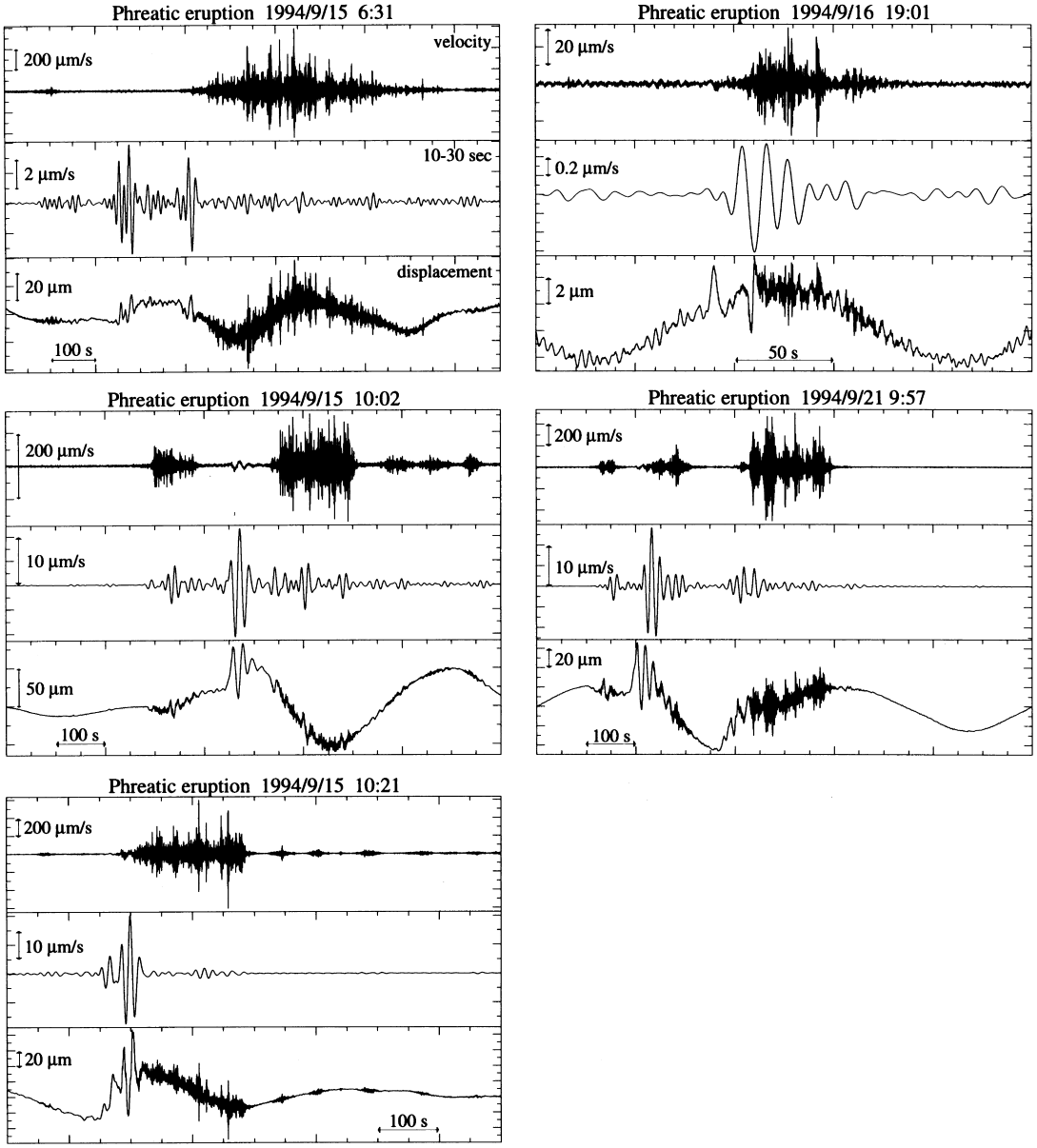

Fig. 11. Broadband seismograms for the phreatic eruptions analyzed. Plots correspond to those shown in Fig. 10(b), but pertain to five other phreatic eruptions listed in Table 4. Note the same general feature of these broadband seismograms as explained in the text (i.e. relative timing and amplitudes of VLPD, LPP, SPT). The LPPs of the event on September 16 are similar in size with LPTs, but still show the characteristics as associated with an eruption. The very long-period oscillations of several hundreds seconds common in the displacement plots are likely due to noise.

where R, ΔP, and μ are the radius of the sphere, pressure change, and the rigidity of the surrounding medium, respectively, and $\lambda = \mu$ is assumed. If we take a radius $R \sim 0.5$ km (as will be mentioned in the next section, we roughly estimate that this is the maximum size of the source) and $\mu = 1.7 \times 10^9$ N/m^2, the estimated pressure change is $\Delta P \sim 6$ kPa for the largest eruption of 9/21 09:55 ($\Delta V = 1454$ m^3, Table 3). Since the

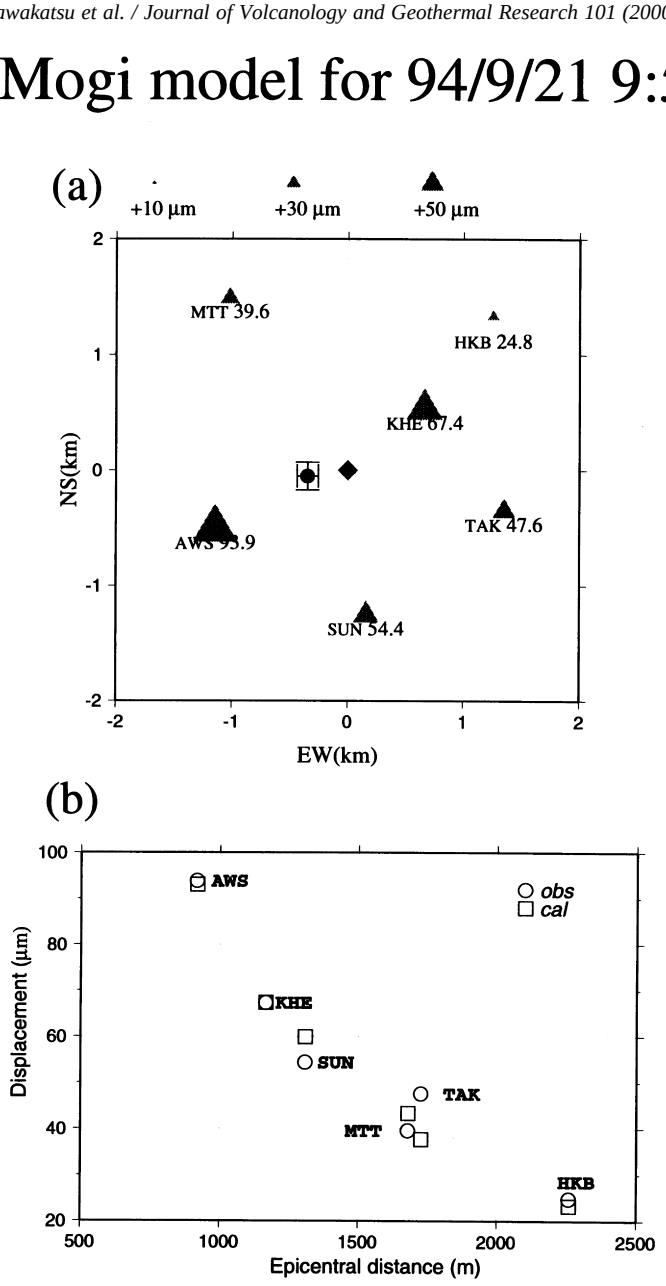

Fig. 12. (a) The vertical heights of VLPDs for the eruption of 9:57, September 21 are plotted in a map view, together with the estimated epicenter of the spherical source. (b) The same data are plotted as a function of the distance from the estimated source (0.35 km west and 0.05 km south of the first crater). Circles are for the data and squares are for predicted values from an isotropic source model (Table 4).

pressure change scales with the inverse cube of the sphere radius, the precise determination of the size is necessary to constrain the pressure change. In terms of the seismic moment, these values give $M_0 \sim 7.4 \times 10^{12}$ Nm (Aki and Richards, 1980), which translates into a moment magnitude of $M_w \sim 1.2$. Although this value appears small, the excitation at long periods ($\sim$20 s) is comparable in magnitude as that of an earthquake of magnitude $M \sim 4$. If we assume a LPT is also due to the same source (i.e. $R \sim 0.5$ km), corresponding

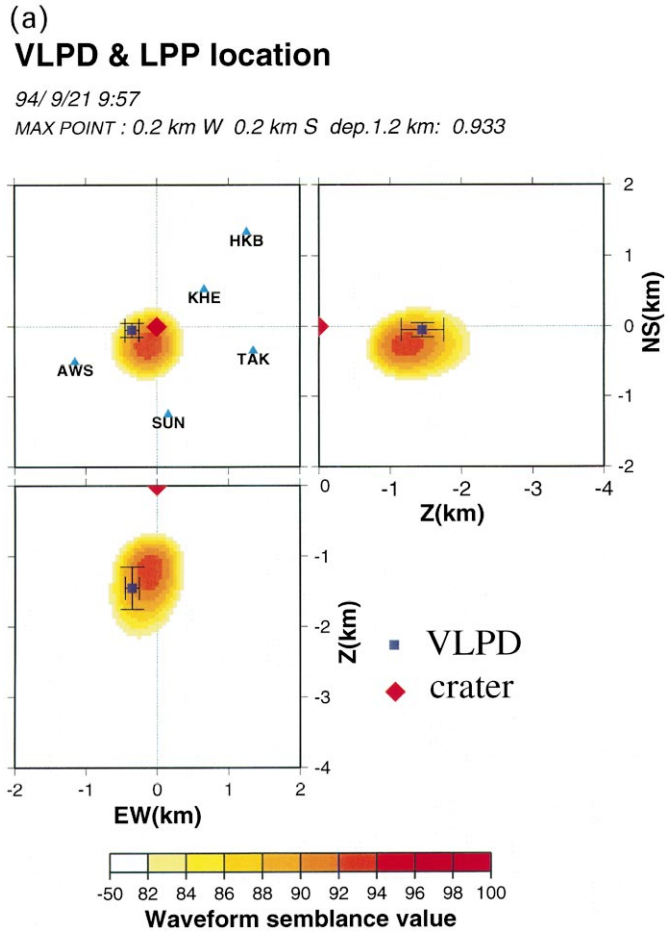

Fig. 13. (a) Estimated source location of the VLPD for the eruption of 9:57, September 21 is plotted against the contour plot for the waveform semblance of the LPP of the same event. The filled diamond denotes the crater. Standard deviation error bars are also plotted for the VLPD source. Both sources are located in the same general area within the error bars. (b) Locations of all the analyzed LPTs (triangles), LPPs (circles), and VLPDs (squares) listed in Tables 2–4 are plotted together, illustrating general agreement in the estimated source region.

Table 4
VLDP source location by Mogi model (locations are given relative to the 1st crater in Table 1)

Date and time	E–W (km)	N–S (km)	Z (km)	ΔV (m^3)	Variance reduction (%)
09/15 06:31	0.20W ± 0.07	0.00S ± 0.10	0.90 ± 0.30	380 ± 41	99.1
10:02	0.25W ± 0.11	0.00S ± 0.14	1.10 ± 0.42	1211 ± 248	98.6
10:21	0.30W ± 0.14	0.10S ± 0.17	1.70 ± 0.53	1261 ± 41	99.2
09/16 19:01	0.30W ± 0.06	0.05N ± 0.08	1.65 ± 0.17	120 ± 14	99.9
09/21 09:57	0.35W ± 0.09	0.05S ± 0.12	1.45 ± 0.31	1454 ± 255	98.9
09/22 12:09	0.15W ± 0.10	0.00S ± 0.12	1.35 ± 0.29	554 ± 91	98.3

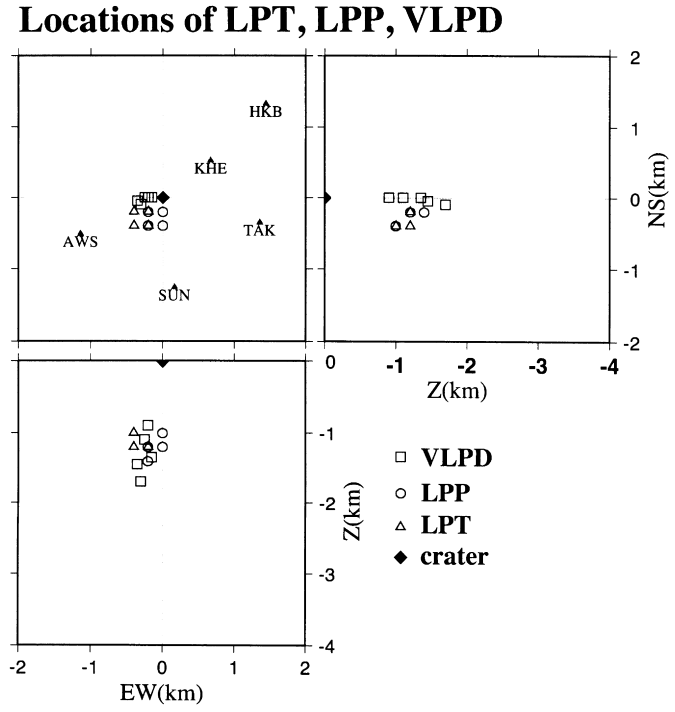

(b)

Fig. 13. (*continued*)

pressure change would be on the order of few 100 Pa. This is a very small fraction of lithostatic pressure (20 MPa) at the same depth.

3.3. Source mechanism

In the preceding analyses to locate the source of long-period signals, we assumed an isotropic (or spherical) source as a first-order approximation. To further constrain the characteristics of the source of the long-period signals, we performed a point moment tensor inversion for LPTs and LPPs (Kaneshima et al., 1996; Legrand et al., 2000 – this issue). Fig. 14 shows the focal mechanism of the deviatoric part of the best moment tensor solutions for LPTs and LPP obtained by Legrand et al. (2000 – this issue) after analyzing long-period part of the data. Although the reliability of these deviatoric components is not very high, they may be interpreted as originating from inflation or deflation of a vertical crack aligned NNW to SSE, parallel or subparallel to the chain of older craters (Fig. 1). The ratio of the isotropic part and the crack part is estimated to be 3.5:1 by Legrand et al. (2000 – this issue).

The steep incident angles at UMN and SUN (Fig. 5), which cannot be well explained by a point source may

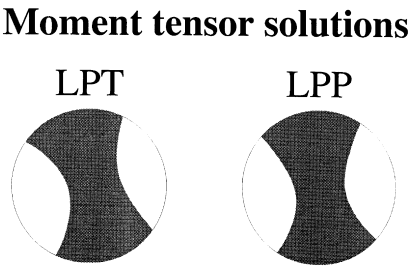

Fig. 14. Moment tensor solutions for a LPT and a LPP determined by Legrand et al. (2000 – this issue). Only the deviatoric part is shown in the lower-hemisphere equal-area projection. (a) LPT at 07:25, November 23; (b) LPP at 10:21, September 15. These deviatoric components are consistent with the presence of a vertical crack trending NNW to SSE, parallel to the chain of the old craters (Fig. 1; see also the text).

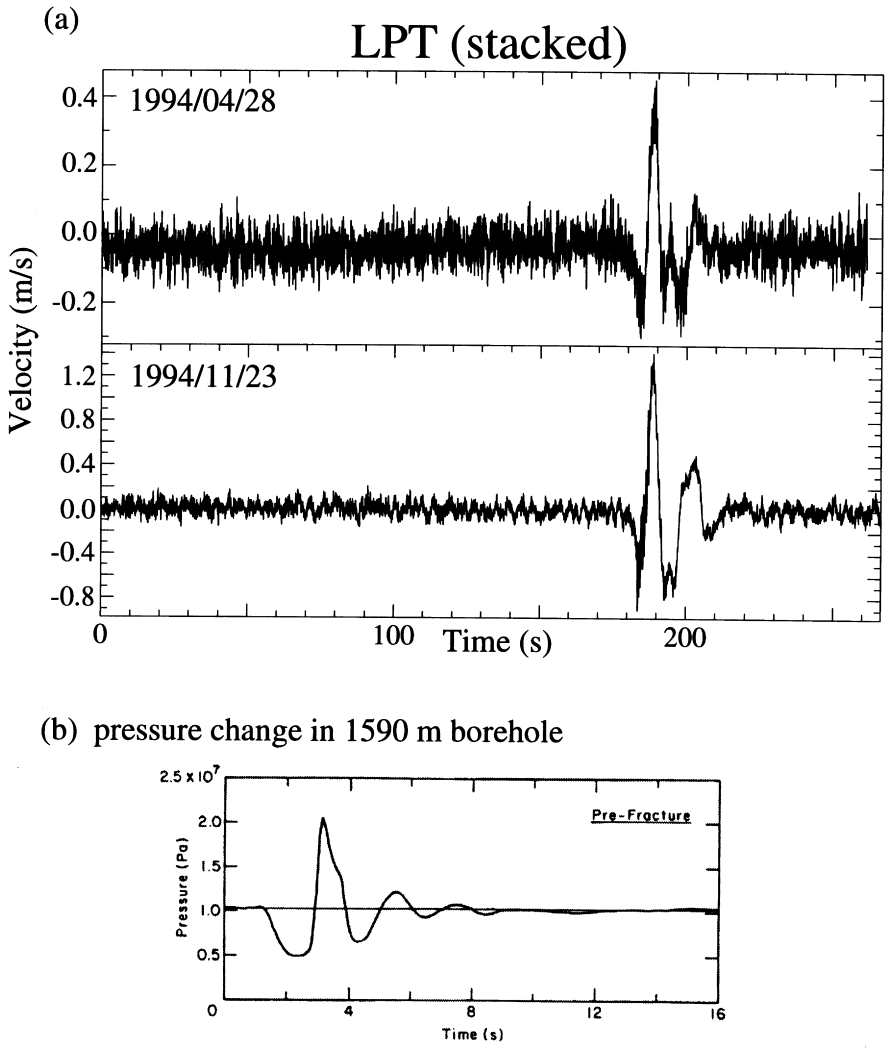

Fig. 15. (a) Stacked LPT seismograms: vertical component broadband velocity seismograms are stacked for more than 100 LPTs which occurred in a single day. Records from two different days are stacked to observe the waveform in raw velocity records. (b) The pressure variation near the surface of a 1590 m borehole due to rapid fluid withdrawal at the surface (after Ferrick et al., 1982). Note the strong similarity of this to the LPT seismograms for Aso shown in (a).

require a finite source. It is found that if the moment tensor source extends to several hundred meters north of SUN and also south of UMN roughly along the chain of older craters, the steep incident angles of the bandpassed waveforms can be explained. The particle motions at other stations around the crater, KHE, AWS, TAK, and HKB are not inconsistent with this finite source model, as long as the point source location estimated with the waveform semblance method above correspond to the centroid location of the moment release.

There is also a systematic misfit in the spherical source model (Mogi model) for VLPD: the observations are smaller than the calculations by 10% or more at stations along the crater chain, SUN and MTT, while those observed at the other stations AWS, TAK, and HKB, are larger (Fig. 12b). This pattern of misfit is similar to that found for LPT, and we

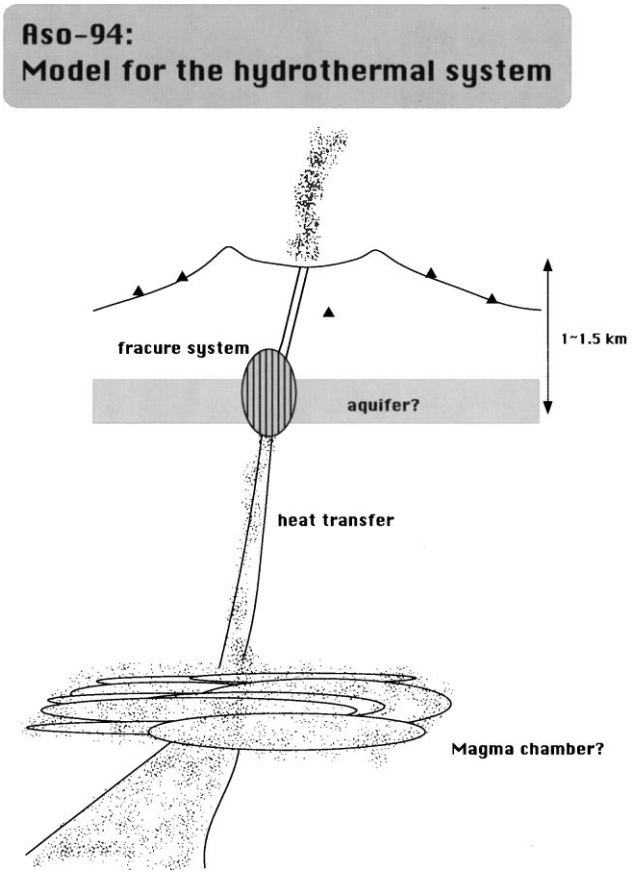

Fig. 16. A cartoon showing our proposed configuration of a hydrothermal system beneath the crater (see text). Neither the aquifer nor the magma chamber is identified via any direct geophysical observation.

find that a class of models corresponding to combination of a NNW-SSE striking vertical crack and isotropic source improves the fit.

All these observations support Sassa's idea of the presence of a crack-like feature in the NNW–SSE direction of the chain of older craters. The lines of evidence are, however, still too weak to be conclusive.

4. Discussion

4.1. Interpretation of the broadband waveforms in terms of a hydrothermal system beneath the crater

Considering that the source locations of LPT, LPP and VLPD determined by different methods are very close (see also Legrand et al., 2000 – this issue), we believe that the source regions are the same. There are some pieces of evidence, which suggest that the source is not a magma chamber. First, the source of LPT and VLPD is shallow (1–1.5 km deep). Second, Aso volcano is in a relatively quiet period (the most recent magmatic event occurred in 1990). Third, the surface temperature of the pond at the bottom of the Naka-dake first crater is only 70°C, and the crater lake has not dried out. It is more plausible that the LPT source is a hydrothermal system including an aquifer and a NNW–SSE trending vertical crack or fractures filled with water and fragmented rocks. The presence of ample water, as well as a system which can quickly circulate the water below the crater, is suggested by the quick changes in the geomagnetic field associated with the activity of Aso volcano (Tanaka, 1993).

Based on our LPT and VLPD observations, we

construct the following qualitative model of the hydrothermal system below the Naka-dake first crater (Kaneshima et al., 1996). Heat is gradually transported upward to the LPT source region from a deep-seated magma chamber in the form of liquid or gas even during a "quiet" period. The source region not only buffers increase in pressure induced by such upward heat transport, but also leaks gas or water further upward to the bottom of the crater lake. Such upward leakage and/or the flow of heat from below often fluctuate and rise suddenly, driving the aquifer and the crack into resonance and resulting in a LPT.

Fig. 15a shows the vertical component broadband velocity seismograms stacked for more than 100 LPTs occurred in a single day. Although it is very difficult to discuss the initial polarity of a LPT in individual raw seismograms, these stacked seismograms clearly indicate the polarity is negative. Fig. 15b shows the pressure variation near the surface of a 1590 m borehole due to rapid fluid withdrawal at the surface (after-Ferrick et al., 1982). Strong similarity of these waveforms supports the interpretation of LPT as a result of the fluid transient out of the aquifer induced by the fluid leakage to the surface as suggested above. Although the observed polarities of LPTs are mostly negative, there appear to be periods during which positive polarities are also observed (September 1994). Considering that a number of phreatic eruptions took place in these periods, presence of positively polarized LPTs may indicate a general increase in the heat transport from the deep magma chamber. If such a relation can be established, we may become able to grasp the condition of the deep magma chamber by monitoring LPTs.

The interpretation of the broadband waveforms observed for phreatic eruptions seems very simple (Fig. 10b). Because of the proximity of the stations compared to the wavelength of the signals, the observed long-period displacement signals (LPP and VLPD) can be considered proportional to the displacement at the source region. The observed positive upward displacement therefore should correspond to inflation of the source region, leading to the following interpretation. A few minutes prior to an eruption, the pressure in the source region gradually increases, exciting (LPP) and inflating (VLPD) the crack and the aquifer. This may occur when heat injection from below increases and stays high for a while, and/or the bottom of the crater lake is shut off by sedimentation of mud. Explosive ejection of gas and mud into the air occurs when the pressure becomes too high to be sustained. Short period tremors are excited when the gas and fluid flow rapidly from the LPT source to the bottom of the crater. This corresponds to the deflating discharging stage. The cessation of short-period tremor corresponds to the end of the ejection, and the source region is deflated back to the original static level. Although the above model is fairly qualitative and needs to be tested against further dynamic considerations, we believe that our interpretation of the observed broadband waveforms is straightforward and plausible to first order. Further interpretation of short-period signals in terms of compressible gas dynamics is noted by Kaneshima et al. (1996). Fig. 16 schematically summarizes the image of a hydrothermal system beneath the crater.

Short-period signals are excited by fluid flow, while the long-period signals are due to the inflation–deflation of the LPT source region; as a whole they comprise the seismic manifestation of a phreatic eruption. Different physics apply at different frequencies and thus the complete volcanic seismic signals are essentially broadband. Seismograms shown in Figs. 10 and 11 clearly demonstrate the essential advantage of broadband seismometry at active volcanoes.

4.2. Long period oscillation of a resonator under the crater

The similarity in waveforms among LPTs (Fig. 4) and the common modal peaks among their spectra (Fig. 6) suggest that LPT represents the response of a resonator driven into oscillation by an impulse. It is, however, difficult to reconcile the observed 15 s period with our estimates of the source volume (perhaps up to 1 km maximum dimension) using standard values of physical parameters such as bulk sound velocities of volcanic rocks (4–6 km/s) and magmatic melt (2 km/s) or water (1.5 km/s). Using these parameters for estimating the size of a harmonic resonator would grossly overestimate the dimensions. For instance, Kubotera (1974) interpreted Sassa's "second kind" tremor with only 6–7 s period as a fundamental mode oscillation of a spherical magma chamber, and estimated the diameter of the chamber to be 4–8 km.

The fundamental period of a fluid sphere embedded in an elastic medium can be given by $T \sim 2\pi R/4.4c$, where R and c are the radius and the wave speed of the fluid, respectively (e.g. Kubotera, 1974; Fujita et al., 1995). Taking $R = \sim 0.5$ km and $T = 15$ s, the wave speed of the fluid in the resonator would have to be about 47 m/s for a spherical source. This number is much smaller than those given above and also smaller than that of vapor ($\backsim$300 m/s); we therefore need a mechanism to reduce the traveling speed of waves trapped in the resonator.

Very slow bulk sound velocity may be realized for a mixture of liquid and vapor. According to Kieffer (1977), the bulk sound velocity of the water–steam mixture can be as low as ~20 m/s under atmospheric pressures. This velocity, however, is strongly dependent upon the pressure condition, which affects the compressibility of the vapor; and under the lithostatic loading at a depth of 1 km (~20 MPa), it approaches that of pure vapor (~300 m/s). The bulk sound velocity of the water–steam mixture also depends on the volume fraction of vesicles filled with steam (Kieffer, 1977). If the dominant period of LPT is really controlled by such vesicles, the fact that the period was very stable throughout one year of our observation may indicate that the volume fraction of vesicle in the water remained approximately constant during one year.

4.2.1. Slow waves in solid–liquid two-phase system

There exist a class of waves in a two-phase system of solid–liquid composite which travel more slowly than either of the sound velocities of pure material comprising the system (i.e. the wave speed can be slower than that of the liquid phase). These waves include the tube wave (Biot, 1952), the so-called Biot's slow wave in a porous medium (Biot, 1956), the so-called crack wave (Chouet, 1986; Ferrazzini and Aki, 1987), and waves in solid–liquid alternating layers (Schoenberg, 1983) (Rayleigh wave and Stoneley wave may also be included in the same class, considering that in the high-frequency limit, all the above slow waves have the same characteristics as an interface wave).

The mechanism for these slow waves may be summarized as follows (Yamamura, 1997; Yamamura et al., 1997): consider the propagation of a plane longitudal wave whose wave length is much longer than the microscopic scale of the medium (e.g. pore size). When the liquid "tries" to contract (or expand) in the passage of a wave, due to the "elastic-coupling" along the solid–liquid boundary, there exists a solution in which the solid behaves out-of-phase with the liquid and so will expand (contract), deforming the boundary in such a way that the liquid "feels" easy to contract (expand), compared to the single-phase case; i.e. for a given amount of displacement in the propagation direction, the actual pressure increment of the liquid phase becomes smaller than that of the pure liquid case. The net effect of this elastic-coupling is to reduce the "effective bulk modulus" of the liquid, and as a result the wave speed becomes slower than that in the pure liquid; the stronger the elastic-coupling, the slower the wave speed. Biot (1956) treated the most general case for an isotropic porous medium, and showed that there exist two types of P-wave, one of which is the Biot's slow wave.

Chouet (1986) showed the presence of waves trapped in a fluid-filled crack which propagate with a phase velocity much slower than the sound velocity of the fluid, the so-called "crack wave", and suggested that it may explain the long-period nature of Sassa's second kind of tremor (i.e. LPT). The nature of this crack wave was further studied by Ferrazzini and Aki (1987), and the out-of-phase characteristics stated above were shown. Consideration of the crack wave would greatly reduce the estimation of the size of the resonator as suggested by Chouet (1986). For instance, according to Chouet's study, a wave with a period of 15 s may be generated by a 1 km long crack which is filled with water with the bulk sound velocity of 1.5 km/s, if the crack thickness is on the order of 1 m. Although the presence of crack-like feature is suggested even from our own work (also Kaneshima et al., 1996; Legrand et al., 2000 – this issue), the presence of the large isotropic component is not consistent with a simple model of a single thin crack.

It may be that an inter-connected fracture system developed in the LPT source region behaves as a "cracked medium" in a similar way in which the inter-connected pore space constructs a porous medium. If such a cracked medium is filled with some fluid, there should exist a slow wave, as Biot's slow wave exists in a porous medium. The degree of the elastic-coupling is controlled by the macroscopic effective rigidity of the solid skeleton, and it in turn

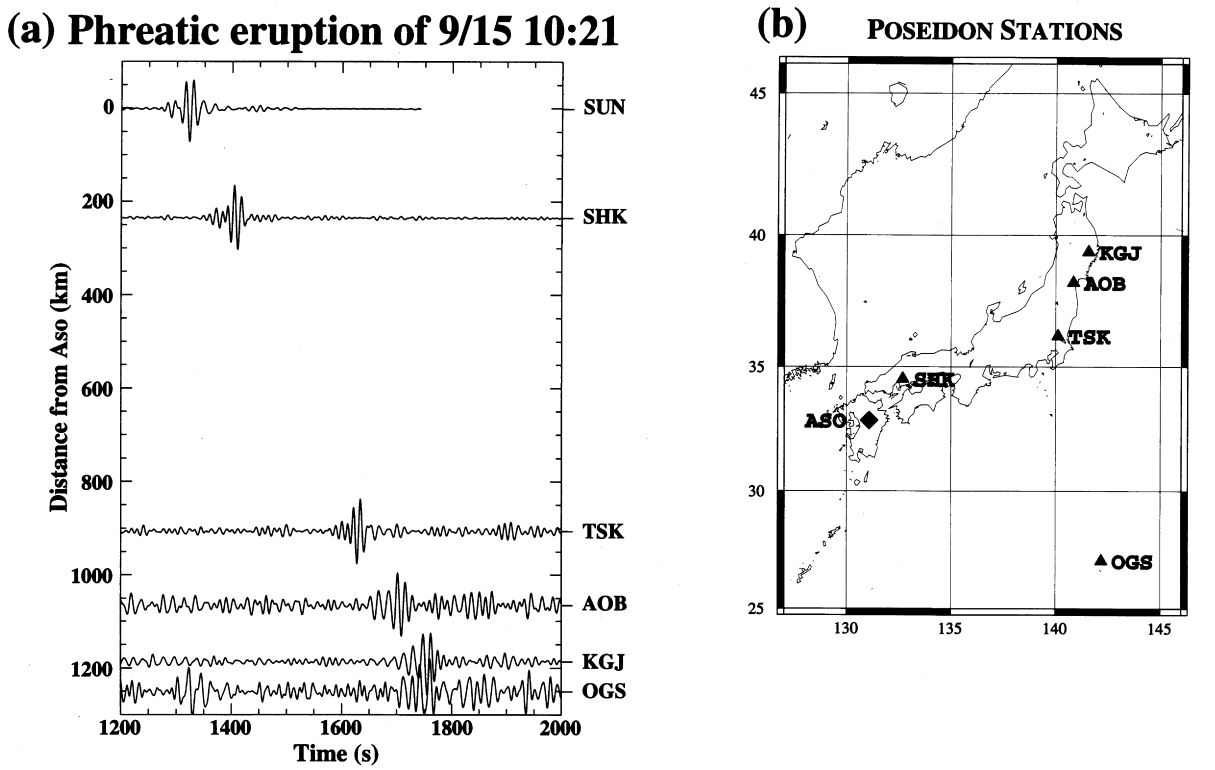

Fig. 17. LPP (10–30 s) seen all over Japan. The LPPs associated with the phreatic eruption of 10:21, September 15 are observed almost everywhere in Japan by the broadband seismometers of the POSEIDON network. (a) Vertical component seismograms are plotted as a function of distance from Aso volcano. The signal can be recognized even at OGS station, situated more than 1200 km away from Aso. (b) Station location map.

controls the velocity of the slow wave (e.g. Johnson and Plona, 1982; Yamamura, 1997). Elastic-coupling in the cracked medium is probably strong, because the skeleton rigidity of inter-connected cracks is likely to be smaller than that of a porous medium with the same porosity. Thus, the slow wave can be very slow, and significant wave energy can exist for the slow wave. Biot's slow wave has never been observed in nature (except in laboratories); if the LPT of Aso is proved to be such a realization, the applicability of Biot's theory in nature becomes also proved.

An attempt to constrain the size and shape of the LPT source is now underway. If the precise size can be estimated, the speed of waves trapped in the source can be estimated. We may then propose a physical model to explain the characteristics of the LPT source, and infer the physical state in the hydrothermal reservoir. The observed high attenuation of LPT also should be remarked. As has been stated earlier, water is the most likely fluid to exist at a depth of about 1 km below the crater, so that viscous drag should not play an important role to dissipate the energy of oscillation. An entirely new mechanism may have to be devised to explain the observed oscillation below the crater.

4.2.2. Realtime monitoring of the volcano

In the nine-month long spectrogram shown in Fig. 6b, the time variation of the amplitude of each mode can be observed. The LPT amplitude appears large in September and November when a number of phreatic eruptions occurred. It should also be noted that the relative amplitude of 15 and 7.5 s modes changes from time to time, although the mode periods do not change noticeably. This can be most likely explained by the change of the location of the excitation source

of LPTs. If the causal relationship between the LPT amplitudes and surface activities can be established, the amplitude information might provide insights into the physical state of the volcano.

The waveform semblance analysis introduced in this paper, or the waveform inversion analysis (e.g. Legrand et al., 2000 – this issue) of LPTs may provide a useful new tool for monitoring the volcano in realtime. Since we know the approximate location of the LPT source, we can "tune-up" the monitoring system (say waveform semblance) to look only at the source region, and to monitor the LPT amplitude. The long-period wavefield can be severely distorted either by surface wave arrivals of teleseismic events or by bad weather (storms in the ocean). In order to distinguish LPTs from this long-period noise, we need several stations surrounding the crater; the semblance value for the noise will be reduced even though the long-period amplitude can be very large. The disturbance due to teleseismic noise is removed as much as possible manually in Fig. 6b.

The LPP and VLPD observed a few minutes prior to the phreatic eruptions (Figs. 10 and 11) might also be used to issue immediate warnings for such eruptions, although the presence of LPP does not seem always to lead to an eruption. One of the surprising observation was that the LPP excited by the phreatic eruption of September 21 (09:57 GMT, Fig. 11) was observed with STS-1 seismometers of the POSEIDON network located all over Japan as far as 1200 km away (Fig. 17). This situation appears very similar to the one reported in our earlier observation in which "10 s waves" are recorded all over Kyushu, although there was no corresponding phreatic eruption at the time (Kawakatsu et al., 1994). If this 10 s wave is excited by a similar mechanism to LPP, the report of Kawakatsu et al. (1994) indicates that there is a case when LPP (or VLPD) is observed but no eruption takes place. In this case, pressure build-up in the LPT source region is insufficient to result in a surface explosion. If we can tolerate such false alarms, immediate warnings for phreatic eruptions may be issued using LPP and VLPD.

4.3. Closing remarks

The activity of Aso volcano changes from time to time and, as stated earlier, our year of observation covers only a relatively quiet period (cf. Fig. 2). It would be extremely interesting to see how the LPT source behaves and what would be recorded by broadband seismometers when real magma comes up and a whole cycle of the activity is monitored with state-of-the-art instruments. Although there is still a lot to be observed for us to fully understand Aso activity, our results so far demonstrate the high potential for broadband seismic observation near active volcanoes to add essential information, which has been missed by conventional seismometry. There is now much evidence from volcanoes of the world indicating the presence of long-period volcanic signals. We feel that volcanology should embrace state-of-the-art developments, and broadband seismometers as well as other instruments, such as infrasonic microphones (e.g. Garces, 1997), should be installed as standard equipment for monitoring volcanic activities.

Acknowledgements

We thank the Aso meteorological station for allowing us to deploy our instruments at its observation sites and for providing various data regarding the surface activity of Aso volcano. We also thank an anonymous referee for the thorough review of the manuscript, and Dr Rick Aster for the useful comments as the editor.

References

Aki, K., Fehler, M., Das, S., 1977. Source mechanism of volcanic tremor: fluid-driven crack model and their application to the Kilauea eruption. J. Volcanol. Geotherm. Res. 2, 259–287.

Aki, K., Richards, P.G., 1980. Quantitative Seismology, Theory and Methods. W.H. Freeman, San Francisco, CA, 932pp.

Aki, K., 1984. Evidence for magma intrusion during the Mammoth lake earthquakes of May and implications of the absence of volcanic (harmonic) tremor. J. Geophys. Res. 89, 7689–7696.

Biot, M.A., 1952. Propagation of elastic waves in a cylindrical bore containing a fluid. J. Appl. Phys. 23, 997–1005.

Biot, M.A., 1956. Theory of propagation of elastic waves in a fluid-saturated porous Solid I. low-frequency range. J. Acoust. Soc. Am. 28, 168–178.

Caloi, P., Lo Surdo, A., Ponte, G., 1948. Agitazioni microsismiche originate da attivita vulcanica. Ann. Geofis. 1, 5–9.

Chouet, B.A., 1985. Excitation of a buried magmatic pipe: a seismic source model for volcanic tremor. J. Geophys. Res. 90, 1881–1893.

Chouet, B.A., 1986. Dynamics of a fluid-driven crack in three

dimensions by the finite difference method. J. Geophys. Res. 91, 13967–13992.

Chouet, B.A., 1996. New methods and future trends in seismological volcano monitoring. In: Scarpa, R., Tilling, R.I. (Eds.), Monitoring and Mitigation of Volcano Hazards. Springer, Berlin, pp. 23–97.

Churei, M., 1985. Particle motion properties and amplitude-frequency distributions of volcanic long-period tremors of Aso volcano, Kyushu (in Japanese). Bull. Volcanol. Soc. Jpn. 30, 71–80.

Crosson, R.S., Bame, D.A., 1987. A spherical source model for low frequency volcanic earthquakes. J. Geophys. Res. 90, 10 237–10 247.

Dreier, R., Widmer, R., Shick, R., Zurn, W., 1994. Stacking of broad-band seismograms of shocks at Stromboli. Acta Vulcanol. 5, 165–172.

Eissler, H.K., Kanamori, H., 1987. A single-force model for the Kalapana, Hawaii, earthquake. J. Geophys. Res. 92, 4827–4836.

Falsaperla, S., Langer, H., Martinelli, B., Schick, R., 1994. Seismic measurements on Stromboli volcano in a wide frequency range. Acta Vulcanol. 5, 173–178.

Ferrazzini, V., Aki, K., 1987. Slow waves trapped in a fluid-filled infinite crack: implication for volcanic tremor. J. Geophys. Res. 92, 9215–9223.

Ferrick, M.G., Qamar, A., St. Lawrence, W.F., 1982. Source mechanism of volcanic tremor. J. Geophys. Res. 87, 8675–8683.

Fujita, E., Ida, Y., Oikawa, J., 1995. Eigen oscillation of a fluid sphere and source mechanism of harmonic volcanic tremor. J. Volcanol. Geotherm. Res. 69, 365–378.

Fukuyama, E., Takeo, M., 1990. Analysis of the near-field seismogram observed during the eruption of Izu-Oshima Volcano on November 16 (in Japanese). Bull. Volcanol. Soc. Jpn. 35, 283–297.

Furumoto, M., Kunitomo, T., Inoue, H., Yamada, I., Yamaoka, K., Ikami, A., Fukao, Y., 1990. Twin sources of high-frequency volcanic tremor of Izu-oshima volcano, Japan. Geophys. Res. Lett. 17, 25–27.

Garces, M.A., 1997. On the volcanic waveguide. J. Geophys. Res. 102, 22 547–22 564.

Hagerty, M., Schwartz, S.Y., Protti, M., Garces, M., Dixon, T., 1997. Observation at Costa Rican volcano offer clues to causes of eruptions. EOS 78, 565 (and also 570–571).

Hasegawa, A., Yamamoto, A., 1994. Deep, low-frequency micro-earthquakes in or around seismic low-velocity zones beneath active volcanoes in northeastern Japan. Tectonophysics 233, 233–252.

Hashida, T., 1990. Long-period micro-tremors observed in the Kyushu district, as excited by volcanic activity of the Aso Naka-dake (in Japanese). Bull. Volcanol. Soc. Jpn. 35, 323–326.

Hellweg, P., Seidl, D., Brotopuspito, K.S., Brustle, W., 1994. Team investigates activity at Mt. Semeru, Java, volcano. EOS 75, 313–317.

Johnson, D.L., Plona, T.J., 1982. Acoustic slow waves and the consolidation transition. J. Acoust. Soc. Am. 72, 556–565.

Julian, B.R., 1983. Evidence for dyke intrusion earthquake mechanisms near Long Valley caldera, California. Nature 303, 323–325.

Julian, B.R., Sipkin, S.A., 1985. Earthquake process in the Long Valley caldera area, California. J. Geophys. Res. 90, 11 155–11 169.

Julian, B., Foulger, G., 1996. Earthquake mechanisms from linear-programming inversion of seismic-wave amplitude ratios. Bull. Seismol. Soc. Am. 86, 972–980.

Kanamori, H., Given, J.W., 1982. Analysis of long period seismic waves excited by the May 18, eruption of Mount St. Helens: a terrestrial monopole?. J. Geophys. Res. 87, 5422–5432.

Kanamori, H., Given, J.W., Lay, T., 1984. Analysis of seismic body waves excited by the Mount St. Helens eruption of May 18. J. Geophys. Res. 89, 1856–1866.

Kanamori, H., Ekstrom, G., Dziewonski, A., Barker, J.S., Sipkin, S.A., 1993. Seismic radiation by magma injection: an anomalous seismic event near Tori Shima, Japan. J. Geophys. Res. 98, 6511–6522.

Kaneshima, S., Kawakatsu, H., Matsubayashi, H., Sudo, Y., Tsutsui, T., Ohminato, T., Ito, H., Uhira, K., Yamasato, H., Oikawa, J., Takeo, M., Iidaka, T., 1996. Mechanism of phreatic eruptions at Aso volcano inferred from near-field broadband seismic observations. Science 273, 642–645.

Kawakatsu, H., 1989. Centroid single force inversion of seismic waves generated by land slides. J. Geophys. Res. 94, 12363–12374.

Kawakatsu, H., Ohminato, T., Ito, H., Kuwahara, Y., Kato, T., Tsuruga, K., Honda, S., Yomogida, K., 1992. Broadband seismic observation at the Sakurajima volcano, Japan. Geophys. Res. Lett. 19, 1959–1962.

Kawakatsu, H., Ohminato, T., Ito, H., 1994. 10 s-Period volcanic tremors observed over a wide area in southwestern Japan. Geophys. Res. Lett. 21, 1963–1966.

Kieffer, S.W., 1977. Sound speed in liquid–gas mixtures: Water–air and water–steam. J. Geophys. Res. 82, 2895–2904.

Kieffer, S.W., 1984. Seismicity at Old Faithful Geyser: an isolated source of geothermal noise and possible analogue of volcanic seismicity. J. Volcanol. Geotherm. Res. 22, 59–95.

Kikuchi, S., 1974. On the long-period volcanic micro-tremors observed at Mt. Aso. Bull. Disast. Prevent. Res. Inst., Kyoto Univ. 17B, 1–8.

Kubotera, A., 1974. In: Civetta, L., Gasparini, P., Luongo, G., Rapolla, A. (Eds.). Volcanic tremors at Aso volcano, Physical Volcanology, Elsevier, pp. 29–47.

Kuwahara, Y., Ito, H., Kawakatsu, H., Ohminato, T., Kiguchi, T., 1997. Crustal heterogeneity as inferred from seismic coda wave decomposition by small-aperture array observation. Phys. Earth Planet. Inter. 104, 247–256.

Leet, R.C., 1988. Saturated and subcooled hydrothermal boiling in groundwater flow channels as a source of harmonic tremor. J. Geophys. Res. 93, 4835–4849.

Legrand, D., Kaneshima, S., Kawakatsu, H., 2000. Moment tensor analysis of near field broadband waveforms observed at Aso volcano, Japan, J. Volcanol. Geotherm. Res. 101, 155–169.

McNutt, S.R., 1986. Observations and analysis of B-type earthquakes, explosions, and volcanic tremor at pavlov volcano, Alaska. Bull. Seismol. Soc. 76, 153–175.

Matsubayashi, H., 1995. Origin of the long-period tremors and long-

period seismic waves preceding mud-eruptions observed at Aso volcano (in Japanese). Master's thesis, University of Tokyo.

Minakami, T., 1960. Fundamental research for predicting volcanic eruptions (Part 1). Bull. Earthquake Res. Inst. 38, 497–544.

Mogi, K., 1958. Relations between the eruptions of various volcanoes and the deformations of the ground surfaces around them. Bull. Earthquake Res. Inst. 36, 99–134.

Neidel, N., Tarner, M.T., 1971. Semblance and other coherency measure for multichannel data. Geophysics 36, 483–497.

Nettles, M., Ekstrom, G., 1998. Faulting mechanism of anomalous earthquakes near Bardarbunga volcano, Iceland. J. Geophys. Res. 103, 17 973–17 983.

Neuberg, J., Lucket, R., Ripepe, M., Braun, T., 1994. Highlights from a seismic broadband array on Stromboli volcano. Geophys. Res. Lett. 21, 749–752.

Nishimura, T., Hamaguchi, H., Ueki, S., 1995. Source mechanisms of volcanic tremor and low-frequency earthquakes associated with the –89 eruptive activity of Mt Tokachi, Hokkaido, Japan. Geophys. J. Int. 121, 444–458.

Ohminato, T., 1997. Broadband analysis of seismic signals observed in and around active volcanos, DSc Thesis, University of Tokyo.

Ohminato, T., Ereditato, D., 1997. Broadband seismic observations at Satsuma-Iwojima volcano, Japan. Geophys. Res. Lett. 24, 2845–2848.

Ohminato, T., Chouet, B., Dawson, P., Kedar, S., 1998. Waveform inversion of very long period impulsive signals associated with magmatic injection beneath Kilauea volcano, Hawaii. J. Geophys. Res. 103, 23 839–23 862.

Rowe, C.A., Aster, R.C., Kyle, P.R., Schlue, J.W., Dibble, R.R., 1998. Broadband recording of Strombolian explosions and associated very-long-period seismic signals on Mount Erebus volcano, Ross Island, Antarctica. Geophys. Res. Lett. 25, 2297–2300.

Sassa, K., 1935. Volcanic micro-tremors and eruption-earthquakes (Part 1 of the geophysical studies on the volcano Aso). Mem. Coll. Sci. Kyoto Univ. Series A 18, 255–293.

Schoenberg, M., 1983. Wave propagation in a finely laminated periodic elastoacoustic medium. Appl. Phys. Lett. 42, 350–352.

Seidl, D., Schick, R., Riuscetti, M., 1981. Volcanic tremors at Etna: a model for hydraulic origin. Bull. Volcanol. 44, 43–56.

Takei, Y., Kumazawa, M., 1995. Phenomenological representation and kinematics of general seismic source including seismic vector modes. Geophys. J. Int. 121, 641–662.

Takeo, M., Hamada, N., Kashiwabara, S., Uhira, K., 1984. Analysis of long-period seismic waves excited by the explosive eruption of Mt. Asama on April 8 (in Japanese). Bull. Volcanol. Soc. Jpn. 29, 31–44.

Takeo, M., Yamasato, H., Furuya, I., Seino, M., 1990. Analysis of long-period seismic waves excited by the November, eruption of Izu-Oshima volcano. J. Geophys. Res. 95, 7–19393.

Takeo, M., 1992. The rupture process of the offshore Ito earthquakes preceding a submarine volcanic eruption. J. Geophys. Res. 97, 6613–6627.

Tanaka, Y., 1993. Eruption Mechanism as inferred from geomagnetic changes with special attention to the – activity of Aso Volcano. J. Volcanol. Geotherm. Res. 56, 319–338.

Uhira, K., Takeo, M., 1994. The source of explosive eruptions of Sakurajima volcano, Japan. J. Geophys. Res. 99, 17 775–17 789.

Uhira, K., Ikeda, S., Takeo, M., 1994a. Source process of explosion earthquakes deduced from short-period records at Sakurajima volcano. Bull. Volcanol. Soc. Jpn. 40, 295–310.

Uhira, K., Yamasato, H., Takeo, M., 1994b. Source mechanism of seismic waves excites by pyroclastic flows observed at Unzen volcano. Jap. J. Geophys. Res. 99, 17 757–17 773.

Wallace, T.C., 1985. A reexamination of the moment tensor solutions of the mammoth lakes earthquakes. J. Geophys. Res. 90, 11 171–11 176.

Wielandt, E., Steim, J.M., 1986. A digital very-broad-band seismograph. Ann. Geophys. 3, 227–232.

Yamasato, H., Fukui, K., Uhira, K., Hashimoto, T., Hori, H., 1993. Analysis of seismic and acoustic signals excited by pyroclastic flows at Unzen volcano (in Japanese). Bull. Volcanol. Soc. Jpn. 38, 79–90.

Yamamura, K., 1997. Slow waves in solid-liquid two-phase systems (in Japanese). Master's thesis, University of Tokyo.

Yamamura, K., Takei, Y., Kawakatsu, H., 1997. Slow waves in solid/fluid systems. Programme and Abstracts, Japan Earth and Planetary Science Joint Meeting., Tokyo (in Japanese).